frontiers in Earth Science

ORIGINAL RESEARCH
published: 28 May 2021
doi: 10.3389/feart.2021.674584

Ongoing Inversion of a Passive Margin: Spatial Variability of Strain Markers Along the Algerian Margin and Basin (Mediterranean Sea) and Seismotectonic Implications

Pierre Leffondré[1], Jacques Déverchère[1], Mourad Medaouri[2], Frauke Klingelhoefer[3], David Graindorge[1] and Mohamed Arab[2]*

[1] Géosciences Océan, Université de Brest, CNRS, Plouzané, France, [2] Sonatrach/Exploration Division, Boumerdes, Algeria, [3] Ifremer, Department of Marine Geosciences, Plouzané, France

OPEN ACCESS

Edited by:
Hector Perea, Complutense University of Madrid, Spain

Reviewed by:
Sierd Cloetingh, Utrecht University, Netherlands
Guillermo Booth-Rea, University of Granada, Spain
Nevio Zitellini, National Research Council, Consiglio Nazionale delle Ricerche (CNR), Italy

***Correspondence:**
Pierre Leffondré
pierre.leffondre@univ-brest.fr

Specialty section:
This article was submitted to Structural Geology and Tectonics, a section of the journal Frontiers in Earth Science

Received: *01 March 2021*
Accepted: *27 April 2021*
Published: *28 May 2021*

Citation:
Leffondré P, Déverchère J, Medaouri M, Klingelhoefer F, Graindorge D and Arab M (2021) Ongoing Inversion of a Passive Margin: Spatial Variability of Strain Markers Along the Algerian Margin and Basin (Mediterranean Sea) and Seismotectonic Implications. Front. Earth Sci. 9:674584. doi: 10.3389/feart.2021.674584

Subduction initiation is an important but still poorly documented process on Earth. Here, we document one of a few cases of ongoing transition between passive and active continental margins by identifying the geometrical and structural signatures that witness the tectonic inversion of the Algerian continental margin and the deep oceanic domain, located at the northern edge of the slow-rate, diffuse plate boundary between Africa and Eurasia. We have analyzed and tied 7900 km of deep seismic reflection post-stacked data over an area of ∼1200 km long and ∼120 km wide. The two-way traveltime lines were converted into depth sections in order to reconstruct and map realistic geometries of seismic horizons and faults from the seafloor down to the acoustic basement. Along the whole length of this young transitional domain, we identify a clear margin segmentation and significant changes in the tectonic signature at the margin toe and in the deep basement. While the central margin depicts a typical thick- and thin-skinned tectonic style with frontal propagation of crustal thrust ramps, the central-eastern margin (Jijel segment) reveals a higher strain focusing at the margin toe together with the largest flexural response of the oceanic lithosphere. Conversely, strain at the margin toe is limited in the western margin but displays a clear buckling of the oceanic crust up to the Spanish margin. We interpret these contrasting, segmented behavior as resulting from inherited heterogeneities in (1) the geometry of the Algerian continental margin from West to East (wrench faulting in the west, stretched margin elsewhere) and (2) the Miocene thermal state related to the diachronous opening of the Algerian basin and to the magmatic imprint of the Tethyan slab tearing at deep crustal levels. The narrow oceanic lithosphere of the Western Algerian basin is assumed to favor buckling against flexure. From the dimension and continuity of the main south-dipping blind thrusts identified at the margin toe, we reassess seismic hazards by defining potential lengths for ruptures zones leading to potential magnitudes up to 8.0 off the central and eastern Algerian margins.

Keywords: subduction inception, Algeria, passive margin, active faulting, seismotectonics, seismic hazard, depth conversion

INTRODUCTION

Inversion of passive margins, although occurring at slow rates and in a subtle way, is commonly reported worldwide and has received increasing attention in the last decades. Actually, passive margins are places of large density contrasts and could therefore be a suitable setting for spontaneous subduction initiation (Cloetingh et al., 1989). Many of them are indeed characterized by post-rift submarine elevated plateaux or underwent recent uplift (Pedoja et al., 2011; Japsen et al., 2012), possibly in response to compressional stresses arising from mantle upwellings related to the Cenozoic collisions (Yamato et al., 2013). However, the conditions required for a tectonic inversion to initiate a subduction appear difficult to meet, as reported in many theoretical or experimental studies (e.g., Cloetingh et al., 1989; Gurnis et al., 2004; Leroy et al., 2004; Nikolaeva et al., 2010; Stern and Gerya, 2018; Cloetingh et al., 2021, and references therein). According to modeling results, several parameters are likely to favor the nucleation of subduction, such as (1) pre-existing mechanical weakness zones in the lithosphere, (2) density contrasts between adjacent plates arising from the thermal state of plates of different ages or from differences in chemical composition and crustal thickness, or (3) changes in relative plate motions. Conversely, several resisting forces are increasing during passive margin evolution, especially plate bending, so that it becomes more and more difficult to initiate subduction as the oceanic lithosphere ages and plate strength increases (McKenzie, 1977; Cloetingh et al., 1989).

Whether a passive margin is prone to focus strain and how the stressed oceanic lithosphere behaves depend on various parameters such as the geometry of the margin, the structure and nature of the continent-ocean transition and the mechanical and thermal properties of the lithosphere (e.g., Nikolaeva et al., 2010; Kim et al., 2018). It appears therefore essential to constrain these parameters in order to try to understand the mechanics of subduction initiation. Yet, owing to the limited number of Cenozoic case studies of subduction initiation at passive margins (e.g., Stern, 2004), the structural and geometrical characteristics of the early stages of subduction are poorly documented.

In this study, we propose to investigate the Algerian margin and its adjacent deep oceanic domain (Western Mediterranean Sea, **Figure 1**) which represent a good example of present-day tectonic inversion in an early stage. This passive margin has suffered from large thrust earthquakes such as the Mw = 6.9, 2003 Boumerdès event (Ayadi et al., 2003) and is experiencing slow-rate crustal shortening at the Africa-Eurasia plate boundary (Bougrine et al., 2019). Several recent studies have shown that the relatively high geothermal gradient of the Algero-Balearic basin (compared to the Liguro Provençal basin) and the deep inherited structures of the eastern and central regions (**Figure 1**) likely contribute to weaken the margin and to focus compressional deformation at the margin toe (Chazot et al., 2017; Hamai et al., 2018; Poort et al., 2020). Several studies in the Mediterranean realm also point to the fact that the inversion may involve the entire oceanic basin and may reactivate pre-existing rift-related structures, such as for instance within the Tyrrhenian and Ligurian basins (Billi et al., 2011; Zitellini et al., 2020; Thorwart et al., 2021). Similar observations have been made in the bay of Cadiz (Gràcia et al., 2003).

In spite of numerous detailed studies led in the last years offshore, no synthetic work has described the evolution of the structural style and of the geometrical properties along the Algerian margin and the deep basin, even if a clear margin segmentation has been reported (Cattaneo et al., 2010; Leprêtre et al., 2013; Khomsi et al., 2019; Strzerzynski et al., 2021). Here we use a large dataset, including seismic lines from different origins to map the most relevant tectonic structures marking the inversion of the Algerian margin: faults, flexure and potentially buckling.

The goals of this study are therefore to (1) identify the major active fault systems by direct and indirect effects imaged on depth-converted seismic sections (**Figure 2**) and (2) image, characterize and compare the main structural features of the submarine fold-and-thrust belt located off Algeria. We also attempt to map the geometry of the oceanic basement and of key seismic reflectors in order to derive the mechanical behavior of the oceanic lithosphere affected by compressional stress and to discuss its flexural state and the distribution of active deformation. Finally, we aim at better identifying the seismic potential of this submarine active fault network using simple scaling relationships between rupture length and estimating magnitudes and the present-day knowledge of historical and instrumental seismicity in coastal Algeria. Indeed, this seismic potential is yet poorly considered in many attempts of seismic hazard mapping owing to the limited knowledge of seismogenic zones offshore (e.g., Boughacha et al., 2004; Ousadou and Bezzeghoud, 2019).

GEODYNAMIC AND SEISMOTECTONIC SETTINGS

The Algerian basin is located in the western Mediterranean Sea which was formed as a consequence of the subduction of the west-Alpine Tethyan slab from late Oligocene to early Miocene (van Hinsbergen et al., 2014, and references therein). The south-westward slab retreat induced the birth of a series of back-arc basins in the European plate, defining a segmented fore-arc known as the AlKaPeCa domain (ALboran, KAbylia, PEloritani, CAlabria; Bouillin et al., 1986). These fragments of the European crust now constitute the internal zones of the Alpine Peri-Mediterranean belts. Peloritan and Calabria blocks migrated eastward, while the Kabylian and the Alboran blocks migrated southward and westward, respectively. They have finally collided with Africa and form the present-day Tyrrhenian, Algerian and north-Morocco margins (Bouillin et al., 1986; Sulli et al., 2021).

According to previous works, the Tethyan slab breakoff and tear started around 17 Ma (Abbassene et al., 2016) in the eastern part of the margin, near the city of Collo (**Figure 2**), and then prograded both eastward and westward (van Hinsbergen et al., 2014). The slab tearing resulted into the post-collisional magmatism found along the Kabylides dated from 17 Ma (Lesser Kabylia) to 11 Ma (Greater Kabylia), affecting both the land area and the adjacent margin (Chazot et al., 2017). Tomographic

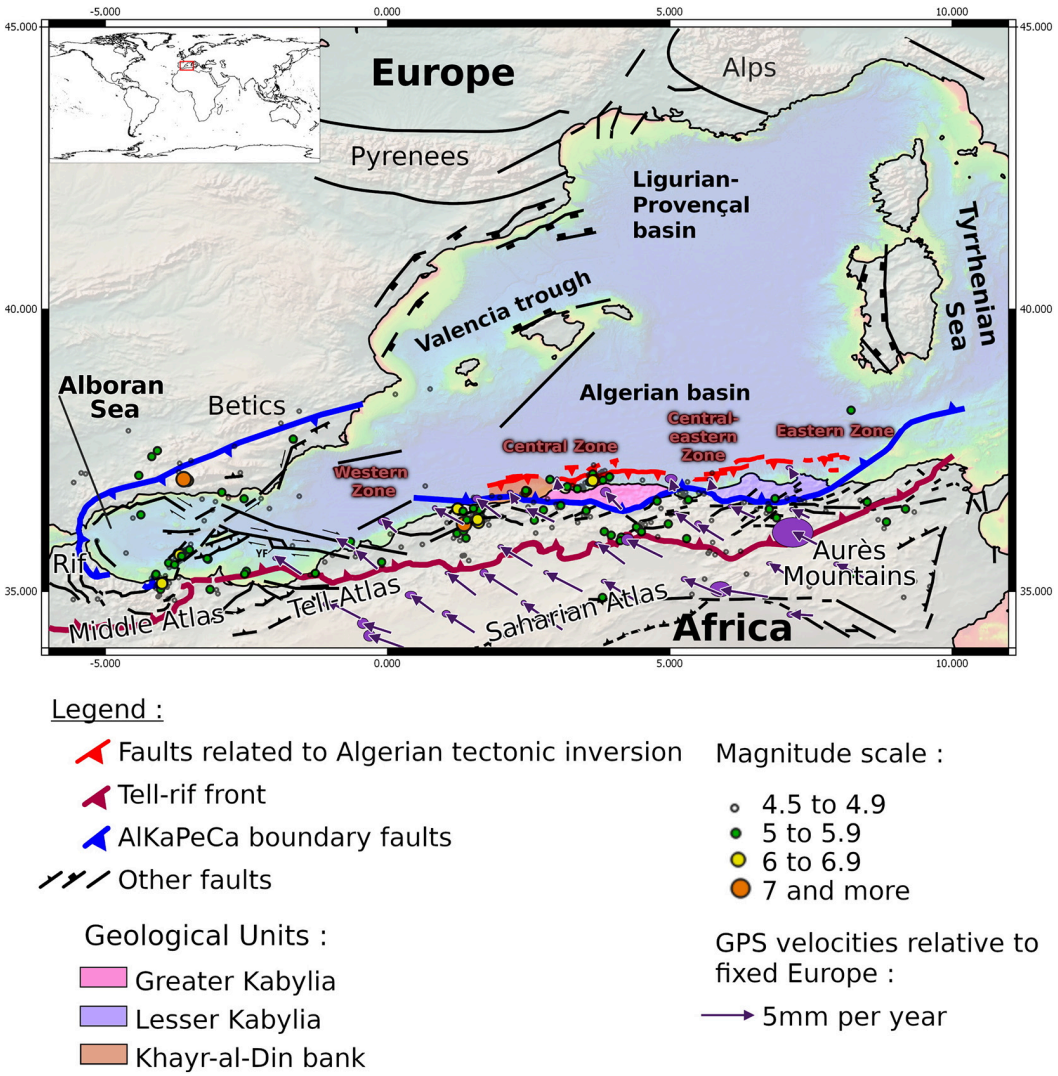

FIGURE 1 | Simplified tectonic sketch of the south-western Mediterranean basins and margins. Blue lines represent the limit between internal and external zones and dark-red lines is the Tell-Rif front. Bright-red lines is a schematic representation of subsurface active faults, redrawn after Yelles-Chaouche et al. (2006), Cattaneo et al. (2010), Giaconia et al. (2015), Rabaute and Chamot-Rooke (2015), Soumaya et al. (2018), and Gaidi et al. (2020). GPS vectors and their associated errors are taken from Bougrine et al. (2019). Circles are M > 4.5 earthquakes taken from the U.S. Geological Survey (2021). YF marks the position of the Yusuf Fault, a notable structure that accommodates the deformation at the transition between the Alboran and the Algerian basins. See text for details.

studies depict a northward dipping slab, detached from the continental crust, at depths between 250 and 660 km under the Algerian basin (Fichtner and Villaseñor, 2015).

The Algero-Balearic basin is considered as a young oceanic domain with a thin oceanic crust and a complex multi-phased opening (Leprêtre et al., 2013; Mihoubi et al., 2014; Bouyahiaoui et al., 2015). The kinematics of opening of the basin is still under debate. Some authors argue for a one-step opening by progressive SE-directed rollback of the Tethyan slab (Gueguen et al., 1998; Jolivet and Faccenna, 2000; Faccenna et al., 2004) from 23 to 8 Ma, while others argue for a diachronous opening during Miocene times (Mauffret et al., 2004; van Hinsbergen et al., 2014, 2020). In the central and western side of the Algerian margin – from Greater Kabilia to the junction with the Alboran domain – recent geodynamical models propose that the subduction first stopped at ca. 17–15 Ma at the docking of the Kabylian blocks with Africa and then propagated eastward and westward owing to a bilateral slab tear (van Hinsbergen et al., 2020). Recent studies of the westernmost Algerian margin (Badji et al., 2015), the Betics and the Rif (Garcia-Castellanos and Villaseñor, 2011; de Lis Mancilla et al., 2015, 2018) have shown that the structure of the southern and northern margins of the Balearic and Alboran basins is characterized by an abrupt transition between continental and oceanic domains, in agreement with a STEP (Subduction-Transform-Edge-Propagator) fault origin (Govers and Wortel, 2005). This slab tear propagation is therefore assumed to have induced, from 16 to 8 Ma, the opening of the central and western Algerian basin along a left-lateral sub-vertical fault, thus forming

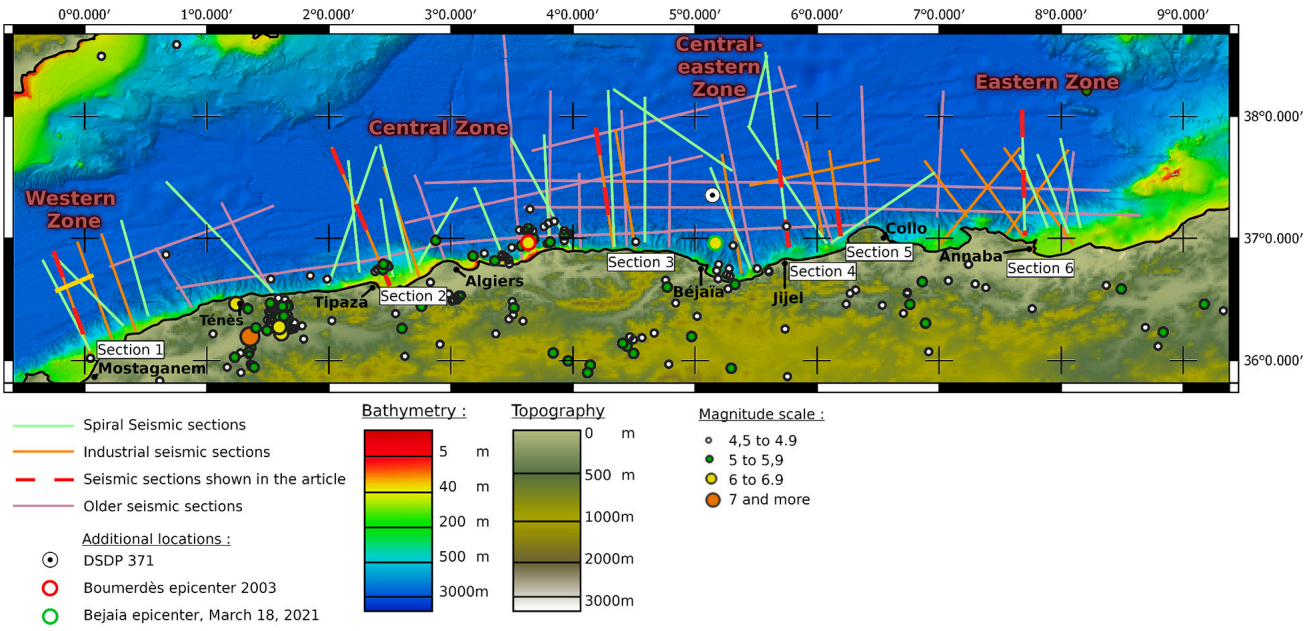

FIGURE 2 | Bathymetry and topography of the Algerian margin, along with the seismic sections which have been depth-converted. Numbered and overlined with red dashes refer to seismic sections partly displayed in this study (see **Figures 4–8**). Circles are $M > 4.5$ earthquakes taken from the U.S. Geological Survey (2021).

a transform-type margin (Medaouri, 2014; Medaouri et al., 2014; van Hinsbergen et al., 2014; Hidas et al., 2019).

The Algero-Balearic basin is supposed to be fully opened at the beginning of the Messinian Salinity Crisis. Since the end of the Tethyan subduction and its subsequent collision, most of the shortening linked to the convergence between Africa and Europe is accommodated in the Maghrebides belt, i.e., the whole Tell-Rif system (Frizon de Lamotte et al., 2009; Bougrine et al., 2019). At the northern plate boundary, this compression has been evidenced by seismic imaging (e.g., Déverchère et al., 2005; Yelles et al., 2009; Leprêtre et al., 2013; Badji et al., 2015; Bouyahiaoui et al., 2015; Arab et al., 2016a,b; Aïdi et al., 2018). From west to east, the Algerian margin appears to be clearly segmented (**Figure 1**):

(1) By contrast with the other margin segments, the steep and linear transform-type margin of the western zone displays very few active faults but is instead characterized by the presence of the Ameur Messinian salt diapir and a laterally continuous post-Messinian trough at the ocean–continent transition (Domzig et al., 2009; Cattaneo et al., 2010; Badji et al., 2015).

(2) The central zone is characterized by the presence of uplifted and tilted blocks along the oceanic transition, like the Khayr-al-Din bank (**Figure 1**), a 15 km thick crust of continental nature affected by an uplift of 0.2 to 0.7 mm/yr during the Plio-Quaternary (Leprêtre et al., 2013; Authemayou et al., 2017). The Greater Kabylia block displays the activation of a backthrust on land and of south-dipping thrusts at the margin toe, suggesting the incipient building of an accretionary wedge (Strzerzynski et al., 2021, and references therein).

(3) The eastern margin (northern flank of the Lesser Kabylia block) has revealed the existence of several deeply rooted thrust ramps located at mid-slope or at the margin toe, sometimes displaying en-échelon pattern at shallow depths, but with little evidence for significant propagation in the deep basin (Kherroubi et al., 2009; Yelles-Chaouche et al., 2009; Mihoubi et al., 2014; Bouyahiaoui et al., 2015; Arab et al., 2016a,b).

Although local strain measurements are lacking, active offshore deformation is clearly evidenced by GPS measurements (Bougrine et al., 2019; **Figure 1**). Up to 4.4 mm/year of shortening is likely accommodated either by faults off Algeria or in regions northwards like in the Betic margin (Giaconia et al., 2015). In the central and eastern Algerian margin (east of Algiers), strain rates are predicted to be less (1.5 mm/year) offshore. However, several $M > 6$ historical (1716 Algiers; 1773 Tipaza; 1856 Jijel) and instrumental (1989 Chenoua; 2003 Boumerdes) earthquakes have revealed submarine sources and have sometimes triggered a tsunami (Yelles-Chaouche et al., 2009, 2017). This active deformation is also expressed by moderate-magnitude, recurrent earthquake activity along the Algerian margin: almost 200 events of magnitude higher than 4.5 are reported since 1952 (**Figure 1**), including six events with magnitudes between 6 and 7.3 (Boughacha et al., 2004; Yelles-Chaouche et al., 2017; Ousadou and Bezzeghoud, 2019).

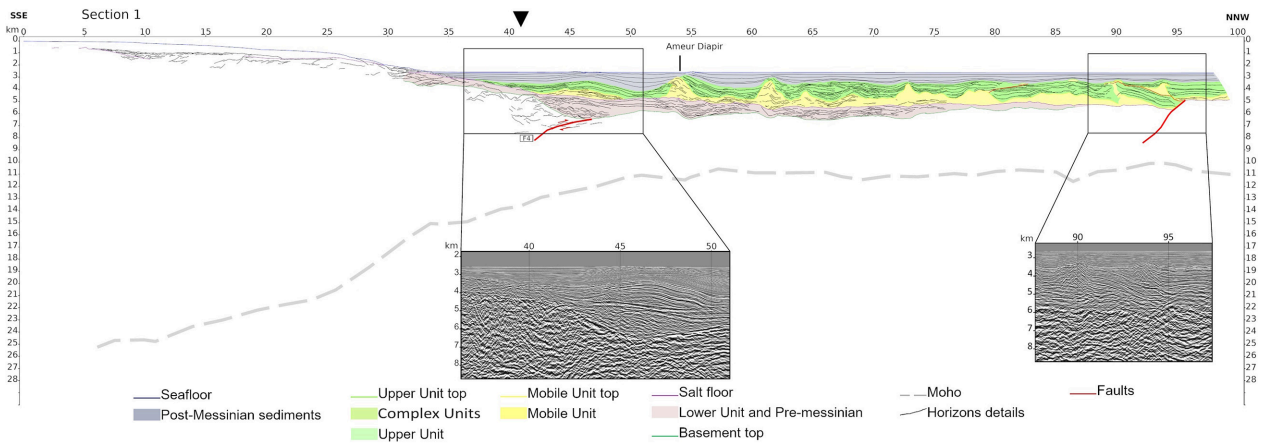

FIGURE 3 | Seismic section 1 (Mostaganem) as a depth-converted line drawing. No vertical exaggeration is present. Major horizons and faults are identified. No major asymmetric basins are identified on this section. The two insets display raw depth-converted extractions of the seismic line. Downward pointing arrow locates the ocean-continent transition.

DATA SETS AND METHODOLOGY

Seismic Data Sets

This study is based upon a compilation of numerous multichannel seismic reflection lines collected in this area over the years. Most of the deep seismic lines from this compilation and the coincident wide-angle and reflection seismic lines were acquired in the scope of the SPIRAL (Sismique Profonde et Investigation Régionale du Nord de l'Algérie) cruise in 2009 aboard the R/V L'Atalante using a 4.5 km digital seismic streamer and a 8909 in3 tuned airgun array (Graindorge et al., 2009). The resulting seismic sections have a low resolution and high penetration owing to the low frequencies of the airguns tuned for combined wide-angle data (**Figure 4A**). We also use some industrial lines published in the last years, designed to image below the Messinian salt layer and the deepest layers of the crust and offering a relatively good lateral and vertical resolution (**Figure 4B**; Cope, 2003). Finally, some older seismic lines from the 1970s are used to improve the coverage of the margin and to tie the main reflectors from one line to another. With the exception of some of the oldest seismic sections, our data are mostly made up of north-south sections that do not cross each other. Profiles with high resolution but low penetration from the 2003 MARADJA (doi: 10.17600/5020080) and the 2005 MARADJA2 (doi: 0.17600/5020080) and SAMRA (doi: 10.17600/5020090) experiments are also used to improve the spatial correlation, but were not used for the depth conversion.

Seismic Processing and Analysis

Seismic reflection imaging of active faults can be a challenging issue (see e.g., Iacopini et al., 2016 and references therein), especially when crustal faults are not offsetting stratal reflections but affect a crystalline basement most often lacking coherent reflections and dominated by scattered energy (Brewer, 1987). Furthermore, artifacts remaining after multichannel seismic processing (especially migration) and recording of out-of-plane reflections are often a source of uncertainties and can lead to misleading interpretations (e.g., Calvert, 2004, 2017; Sibuet et al., 2019).

In our study, all seismic profiles were processed (in two-way-travel time only) as part of previous studies (Leprêtre et al., 2013; Mihoubi et al., 2014; Badji et al., 2015; Bouyahiaoui et al., 2015; Aïdi et al., 2018). A total of 103 seismic profiles were included into this analysis and 156 intersections between the main seismic sections were used to tie the reflectors picked in adjacent profiles. Unfortunately, the oldest seismic lines are lacking resolution, especially below the basement, limiting the amount of horizons that can be correlated when they were the only crossing sections

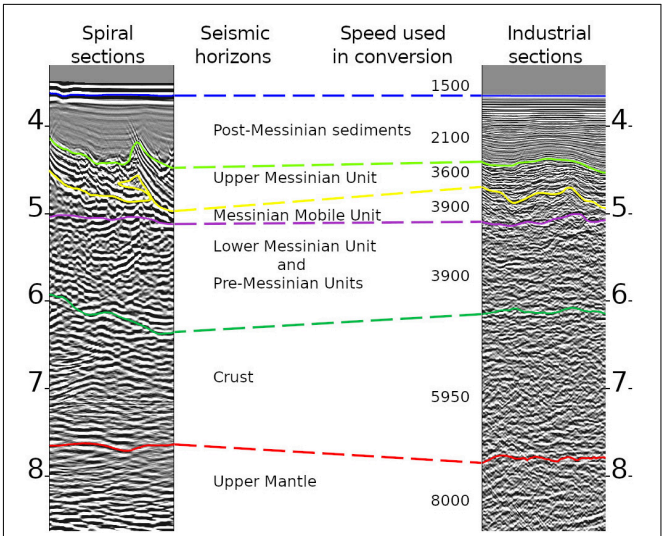

FIGURE 4 | A comparison of the seismic facies identified on SPIRAL **(left)** and industrial **(right)** sections in the deep Algerian basin. Vertical scales are in two-way-travel time and velocities in m/s. Velocity law modified after Leprêtre (2012); Bouyahiaoui (2014), Mihoubi (2014); Arab (2016), and Aïdi et al. (2018).

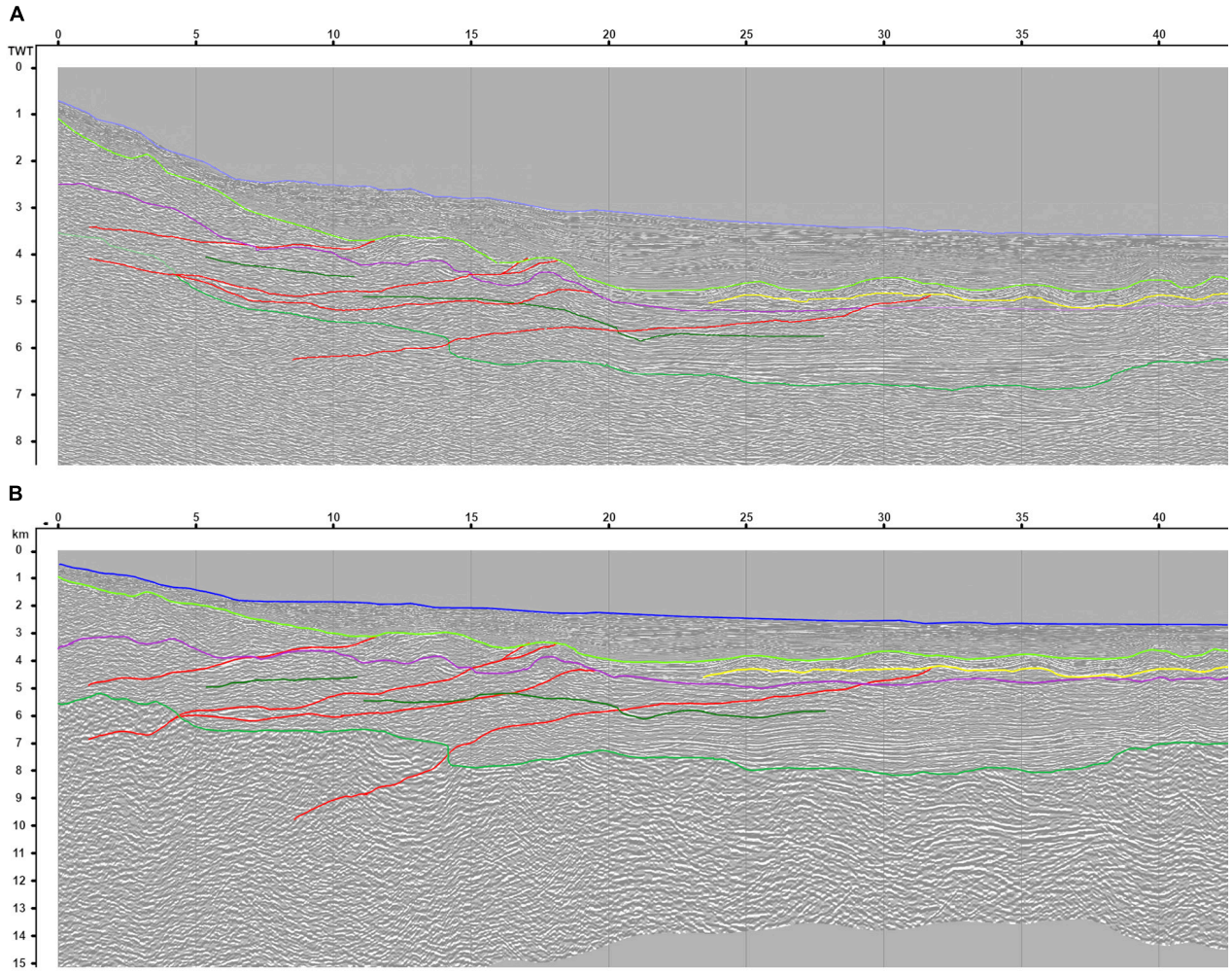

FIGURE 5 | Extraction of Section 5 (East Jijel, Lesser Kabylia, **Figure 2**) without **(A)** or with **(B)** depth conversion and how it modifies the perception of the true geometry of the faults and of the seismic reflectors of the margin.

available. Along the margin, we also used sections from the MARADJA seismic experiments. They are of high resolution, but penetrate only down to the Upper (UU), Mobile (MU) or sometimes lower (LU) Messinian units. Since their contribution in this work is limited, we did not include them on our data location map (**Figure 2**) to avoid overwriting. All sections were visualized and analyzed using the Kingdom Suite© seismic and geological interpretation software. The main reflectors (**Figure 4**) were first interpreted along time sections, and then converted to depth via a simple velocity model, with fixed seismic wave velocities assigned to each layer.

Time-to-Depth Conversion of the Seismic Sections

Our study area displays significant structural and geometrical differences resulting from various effects such as mechanical flexure, subsidence linked to sediment loading and inherited structural features of the continental margin and oceanic domain. In this context and as shown in **Figure 5** and **Table 1**, a time-to-depth conversion is required to improve the structural interpretation and the characterization of the tectonic style (Totake et al., 2017).

For this study, detailed velocity information was available only for a few seismic sections. Most of them originate from the five wide-angle seismic profiles of the SPIRAL project (**Figure 2**). As the five SPIRAL profiles did not allow us to propose a velocity model spanning the complete margin, we have used a simple depth-conversion approach, with a mean velocity being applied to each major unit, allowing us to benefit from a large amount of depth-converted profiles to perform a structural validation.

In detail, we base our time-to-depth conversion over velocity models published in previous studies in the area region and resulting from the processing of the wide-angle SPIRAL lines (see Leprêtre, 2012; Bouyahiaoui, 2014; Mihoubi, 2014; Arab, 2016; Aïdi et al., 2018 for a detailed description of the data processing and modeling). The review of available data shows quite consistent velocities for equivalent sedimentary layers

TABLE 1 | Velocity model used for the depth conversion.

Unit	Velocity in m.s-1
Water	1500
Post-Messinian deposits	2100
Messinian Upper (UU) and Complex (CU) Units	3600
Messinian Mobile Unit (MU)	3900
Messinian Lower Unit (LU) and pre-Messinian deposits	3900
xCrust	5950
Mantle	8000

across the Algerian margin. The depth of the main horizons was then compared to depth-converted sections calibrated by well-constrained depth conversion methods applied along the wide-angle seismic profiles. We use seven velocity layers corresponding to major unconformities and discontinuities observed across the MCS sections (**Figure 4** and **Table 1**). After the conversion, we did an additional check of the interpretation made in our seismic sections, concentrating on the artifacts detected on the depth-converted profiles, and re-ran the depth conversion after slight modifications of our two-way-traveltime pickings. This was important for understanding fault geometry and correcting artifacts caused by more complex geometries like salt-diapirs and arising from the use of constant velocities for each of the seven layers. Indeed, as changes in the picking of the horizons modify the result of the depth conversion, back and forth between picking in two-way-time and depth conversion allowed us to reduce the presence of artifacts.

Although local velocity variations can create deviations of up to 200 m at a given point when compared with the depth-migrated sections found in literature, we have checked that they preserve the overall geometry of reflectors. Our model is calculated from the shallowest to the deepest horizon. The deeper the layer, the more its mapping is sensitive to the differences between the true seismic velocity and our average seismic velocity. These uncertainties remain mostly local, and often associated with Messinian salt diapirs. In the absence of such structures, the depth-converted horizons conform to previous depth-converted data from the wide-angle seismic profiles of the SPIRAL project. To avoid misleading interpretations of the basement/sediment deformations potentially caused by diapirism, we were also careful to discard the short wavelengths (few kilometers) associated with diapirs in our interpretations and only report on longer wavelengths (**Table 2**).

Finally, this time-to-depth conversion approach, in spite of obvious intrinsic limitations, allowed us to obtain for the first time a set of depth maps of major layers based on 59 depth converted seismic sections spread over the Algerian margin and adjacent basin (**Figure 5**).

Faulting Identification

In order to use with caution our data set and avoid misleading interpretations of the fault system along each seismic section, we have used the following five criteria to identify faults:

(a) The first one is a direct identification of the fault trace in the seismic section after processing. The resolution of our data is not always high enough and wrong/erroneous detection are still possible (see section "Seismic Processing and Analysis"). However, by the depth conversion of major seismic units in the reconstruction of a more realistic

TABLE 2 | Synthesis of the information regarding the deformation of the Algerian margin and basin in relation with the tectonic inversion.

	West	Central-West	Central	Central-East	East
DCF at the Basement top					
Minimal half-length	53 km	N.O.	43 km or 90 km	150–170 km	60 km
Minimum amplitude	1,5 km (unconfirmed nature)	N.O.	1,2 km or 1,6 km	2 km	1,5 km
DCF at the Upper Unit top					
Minimal half-length	46 km	67 km	77 km	150–170 km	60 km
Minimum amplitude	0.8 km (unconfirmed nature)	0.9 km	0.5 km	0.6 km	0.5 km
Buckling or short-range undulations					
Average length	35 km	30–40 km	N.O.	N.O.	25 km
Amplitude	0.8 km–1 km	0.9 km	N.O.	N.O.	0.9 km
Faults					
Faults in the continental slope	1	3–4		3	3–4
Highest minimum length	68 km	83 km	175	120	66 km
Faults in the basin	1 reactivation	Disparate observations		N.O.	3
Highest minimum length	13 km	50 km	40 km	N.O.	40 km
Other					
Magnetic anomalies	Non-compliant	Non-compliant	Partially compliant in regard to Hannibal High	Non-compliant	Conform with faults and buckling
Volcanism	Abrupt transform margin		Hannibal high	potential sealed volcano west of the flexural basin	Previously identified volcanism, related to the Collo massif

DCF = downward concave flexure.

spatial relationship of the reflectors, we were able to add a further check on the identification of the faults.

(b) The second criterion is a clear offset of seismic horizons or sharp depth variations. This is a direct indication of the tectonic activity, reflecting the displacement along the fault.

(c) The third criterion is the presence of asymmetric basins (wedge-shaped basins) and/or folding and growth of strata during the development of thrust-related anticlines. These indirect markers of fault activity are widely used in frontal regions of thrust wedges with slow deformation rate (e.g., Tavani et al., 2015 and references therein) and are indeed illustrated in our case study, where sedimentation rates are high enough to record the deformation.

(d) The fourth criterion is the existence of a perturbation at the seafloor. Previous studies have shown that although many thrusts are blind, witnesses of active deformation at the seafloor are locally found in the Algerian offshore (e.g., Déverchère et al., 2005; Domzig et al., 2009; Kherroubi et al., 2009; Cattaneo et al., 2010; Babonneau et al., 2017), therefore we have tried to systematically correlate this shallow deformation with strain markers identified on seismic lines.

(e) The last and more disputable criterion used is salt tectonics as indirect indicator when present. Salt tongues, squeezed diapirs or ramps of the upper units embedded with salt can still be used in some cases to help to evidence the fault activity (e.g., Camerlenghi et al., 2009; Matias et al., 2011; Soto et al., 2018) even if the uplift of the margin by tectonic inversion is also a potential source for salt gliding, as observed in many passive margins (Brun and Fort, 2011).

We assign the highest level of confidence to faults identified based on at least four among the five criteria above. Faults validated by at least three of them, but without an obvious fault trace, are displayed as dashed lines. These faults are supported by strong evidence, but their exact location, lateral continuity and dip value are uncertain. Faults based on fewer criteria are shown as dashed lines with more widely spaced dashes and represent our third and least certain category, while still being supported by evidence along seismic sections.

Concave Flexure and Buckling of the Oceanic Crust and Lithosphere

The detection and the definition of the flexural behavior of the oceanic lithosphere in the region offshore Algeria were not addressed until now and are among the main targets of our study. Hamai et al. (2015) have shown that isostatic anomalies of the area can be interpreted by opposite flexures of two plates separated by a plate boundary located close to the margin toe, resulting from the stress induced by the Europe-Africa convergence. Interestingly, their 2D mechanical modeling predicts a downward bending of the oceanic plate against the continental plate of several kilometers amplitude, with the highest value at the southern tip of the ocean-continent transition and in the central margin. We therefore expect to find evidence for a downward concave flexure (hereafter called DCF) by mapping the various seismic horizons identified over the deep domain. As the distance imaged by our seismic sections, located roughly perpendicular to the coastline, is relatively short (∼200 km, **Figure 2**), the characteristic wavelength of the flexural response and the amplitude of the bulge could be underestimated (Hamai et al., 2015), therefore we only propose a minimal half-wavelength of the DCF associated with minimal amplitudes and lateral extents.

Buckling (or folding) of the oceanic lithosphere is another expected effect of compressional reactivation that is indeed observed coincidently with underthrusting, faulting and prior to subduction initiation (e.g., Stein et al., 1989; Kim et al., 2018). Buckling may occur at crustal or lithospheric levels, depending on the coupling between the upper crust and the lithospheric mantle (Cloetingh et al., 1999; Burov, 2011). It is expressed by undulations of oceanic basement and overlying sediments with a wavelength depending directly on the thickness of competent layers within the oceanic plate (Burov and Diament, 1995; Burov, 2011). In our case study, we rely on the geometry of the basement top and of the salt base to identify this process by the half-wavelength and the amplitude of each undulation. Since inherited irregularities of the basement top may sometimes mimic crustal buckling, we have systematically compared the shape of both reflectors to avoid misleading interpretations. Note that in spite of the limited lengths of some of our profiles (**Figure 2**), lithospheric folding can be characterized here and may be superimposed to the downward flexure of the oceanic lithosphere.

RESULTS

We summarize here the main results of the correlation between seismic sections within different zones of the Algerian margin from west to east (**Figure 2**). We rely on representative seismic sections (**Figures 3**, **6**–**8**) and interpolated maps (**Figures 9**, **10**) as well as on previous results. We use as markers the reflectors identified on **Figure 4** and their lateral continuity maps for the Basement, the MU base and the UU top. Note that on the continental margin, UU and MU generally undergo a lateral transition toward another unit, much thicker (from x2 to x5 thickness, depending on the place considered) and with typically more or less chaotic facies (**Figure 6**) (Déverchère et al., 2005; Strzerzynski et al., 2010, 2021; Lofi et al., 2011a,b; Arab et al., 2016a,b), hereafter labeled "CU" for Complex Unit. We also compare these maps with magnetic data, as they image the structure of the crust (**Figure 10**), and gravimetric data, as gravimetric anomalies may be another indication of crustal flexures.

Western Zone (Mostaganem Region)

Location and Overall Structure

The western zone of the study area corresponds to the Mostaganem region and its transform-type margin which displays an abrupt ocean-continent transition developed during the STEP fault formation (Badji et al., 2015). Here, the Moho depth varies from 22.5 km to 12.0 km depth over a distance of only 27 km (**Figure 3**).

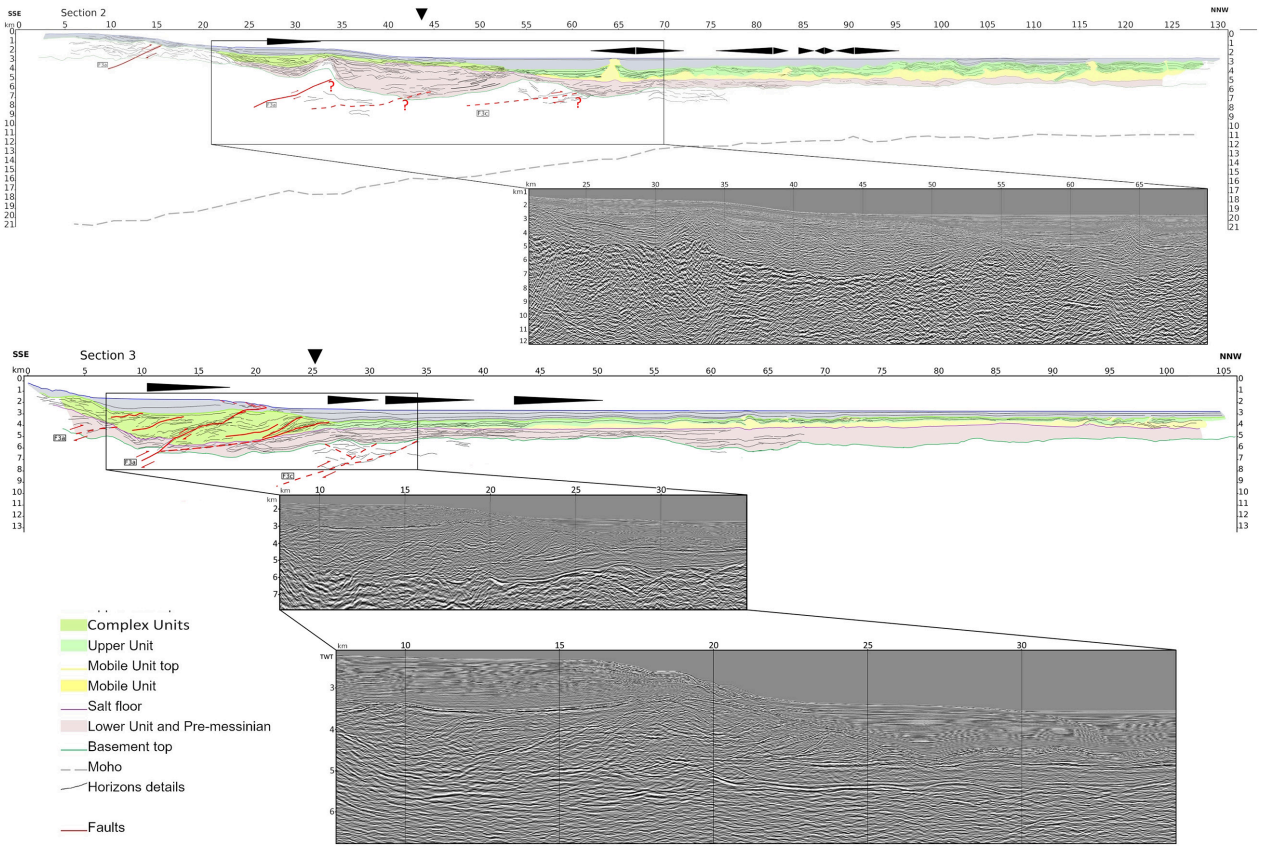

FIGURE 6 | (Right) Seismic Section 2 (Tipaza) as a depth-converted line drawing. No vertical exaggeration is present and faults are identified, as well as major asymmetric basins. The inset displays a raw depth-converted extraction of the seismic line. **(Left)** Seismic Section 3 **(Greater Kabylia)** as a line drawing. No vertical exaggeration. Major horizons and faults are identified, as well as major asymmetric basins. Inset displays a raw depth-converted extraction of the seismic line. The inset on the second line is an extraction of the two-way-time section provided to better evidence faults-related shifts and the deformation of the sediments. Light green unit in the margin corresponds to the Messinian Complex unit (CU) coeval to UU and deposited in response to the major sea level drop of the Messinian Salinity Crisis. Stretched black triangles underline post-Messinian depocenters of sub-basins and their potential asymmetry (wedge-shaped sedimentary units or growth strata) which is assumed to evidence a tectonic control by underlying blind flat-ramp thrusts. Downward pointing arrows locate the ocean-continent transition.

The pre-Messinian units are forming a narrow basin at the margin toe (km 46). The depth-converted seismic sections (**Figure 3**) and depth maps (**Figure 9**) suggest up to 1500 m of pre-Messinian and lower-Messinian sediments and a progressive thinning of these units toward the North, until km-85 where the presence of the pre- and lower Messinian sediments are not anymore detectable. This could be related to a late opening of this basin, i.e., between 11-8 Ma (Mauffret et al., 2004; Booth-Rea et al., 2007, 2018; Medaouri et al., 2014). Section 1 (**Figure 3**) also shows a progressive increase in the depth of both the basement and the base of the salt from the basin toward the coastline from km-87 to km-65 (Section 1, **Figure 3**).

Seismic Section 1

If we discard local, short wavelength changes of the salt base associated with diapirism that we suspect to be artifacts, we observe an undulation of the oceanic basement (between km-45 and km-65, **Figure 3**), suggesting a half-wavelength folding of the crust of ca. 10 km. The southward dipping reflector around km-47 may define the only active fault identified near the margin toe on the three westernmost seismic sections. The abrupt basement transition from 4.7 km to 6.7 km depth between km-42 and km-47 supports the opening of the basin along a strike-slip fault system, indicating the presence of a STEP-margin (Badji et al., 2015).

The westernmost area displays a local thickening of the sedimentary layers of 1.5 km along 53 km distance, from the margin toe to the end of the seismic section. The basement top reaches its deepest point at 6.7 km depth at the margin toe, while its average depth stays at 5.4 km further north in the basin. This corresponds to a thinning of the lower sedimentary unit. The salt base displays a wavy pattern over ca. 35 km, from km-60 to km-95. Even if this wavy aspect may result from small deviations related to internal velocity variations from the salt and overlying sediments, we suggest that they can still be of tectonic origin. In fact, this undulation is bordered by an ancient fault on the north-western part of the area. This fault, previously proposed by Soto et al. (2018), is supposed to be an older structure, evidenced in the basement and re-activated by the compression. It is related to a ramp in the MU and UU. It does not affect the post-Messinian

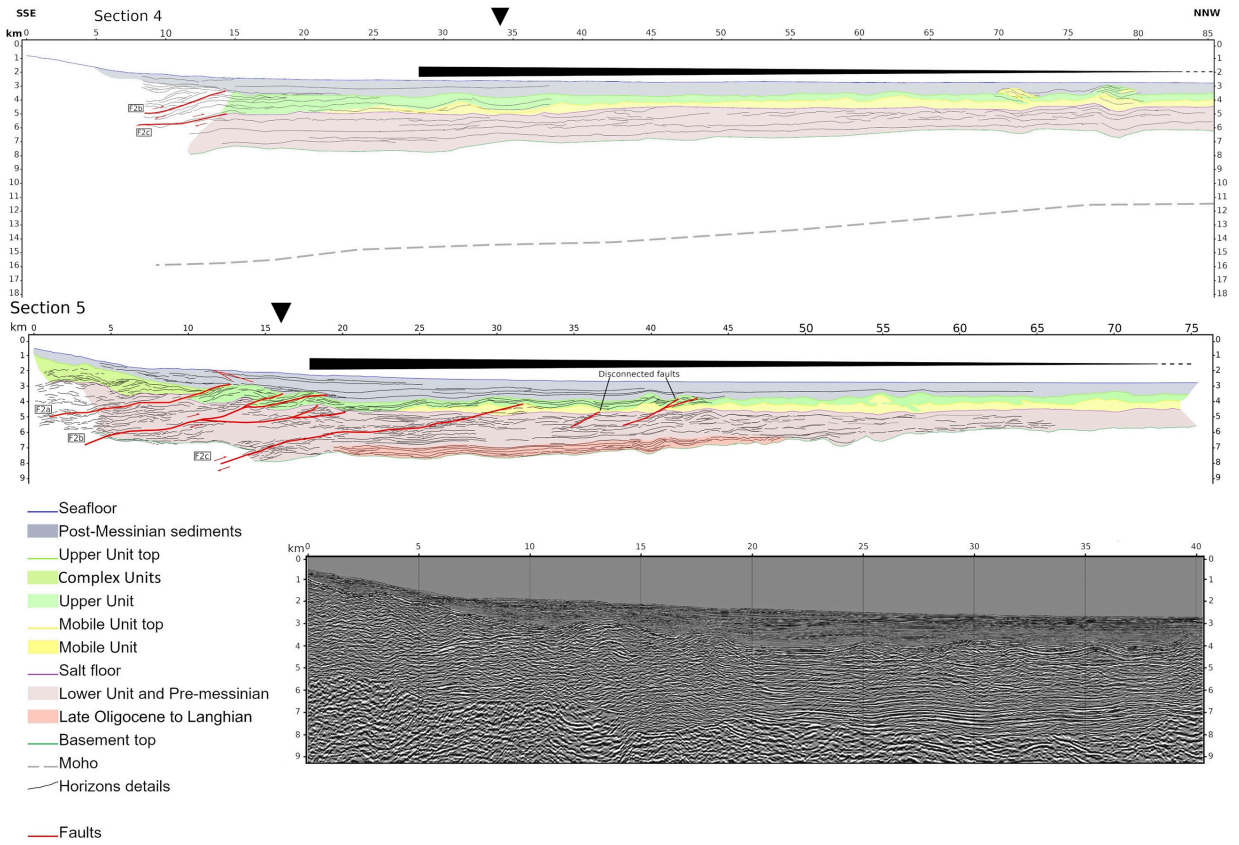

FIGURE 7 | Seismic Section 4 (southern half of the seismic section only) and 5 (continental margin only) **off Jijel**, as depth-converted line drawings. No vertical exaggeration is present. Major horizons and faults are identified, as well as major asymmetric basins. Section 4 evidences the flexure of the basin; its reduced length is due to both the great length of the profile and the absence of any significant geological feature on the second half of the profile with the exception of the global deepening of the horizons toward the margin. Section 5 resolution is higher than the one of Section 4 and goes further onto the continental margin, but it is also shorter and has thus been integrated only to display the faulting system. Light green unit in the margin corresponds to the Complex unit (CU) coeval to UU and deposited in response to the major sea level drop of the Messinian Salinity Crisis. Stretched triangle: same as **Figure 6**. Downward pointing arrow locates the.

sediment directly as the MU constitutes an efficient decoupling layer, but diapirism related to the ramp is visible (**Figure 3**). However, the bathymetry remains undisturbed at the scale of our section. This suggests a folding with a half-wavelength of 15–20 km along the whole margin, with an amplitude of ca. 500 m. We observe no sign of a DCF.

The MU and UU reach a thickness of 1.9 km in the basin, which decreases to 1.1 km at the margin toe. On the upper part of the sedimentary cover, post-Messinian sediments are affected by salt diapirism, creating a basin between two diapirs that stands above the deepest part of the pre-Messinian basin and a secondary and thinner basin northward, again delimited by two diapirs (from km-54 to km-62) (Badji et al., 2015). It is likely that diapirism is responsible for this recent basin, as three salt walls (respectively at 54, 62, and 74 km), including the Ameur diapir (km-54), are observed in this area, with a notable salt weld southward bringing together the UU and LU (**Figure 3**, km-50). Although sediments at the bottom of the pre-Messinian unit are slightly deformed, this tectonic activity remains limited and localized at or near the ocean-continent transition, where we suspect the existence of a steep south-dipping thrust (**Figure 3**).

This fault (F4 on **Figures 3**, **11**) is the only fault directly related to the tectonic reactivation evidenced along this part of the margin. It is more visible on the easternmost seismic sections of the area. The upward movement of the margin relative to the basin would destabilize the MU, favoring its lateral migration by gravity-driven processes and the formation of both the diapirs and the post-Messinian sedimentary basins.

Other inversion-related structures have been described further west, most notably the Yusuf fault which probably affect both the basin and the margin (Martínez-García et al., 2011; Medaouri et al., 2012; Perea et al., 2018; d'Acremont et al., 2020; de la Peña et al., 2020).

Interpolated Maps

A narrow and elongated sedimentary basin is identified at the margin toe above both the basement, the base of MU and the top of UU, and extends at least 70 km along strike (**Figures 9**, **10**). It corresponds to a clear limit of elongated anomalies, both magnetic (**Figure 10B** after Medaouri, 2014) and gravimetric (Badji, 2014) that is proposed to underline the ocean-continent transition (Badji et al., 2015). As previously reported

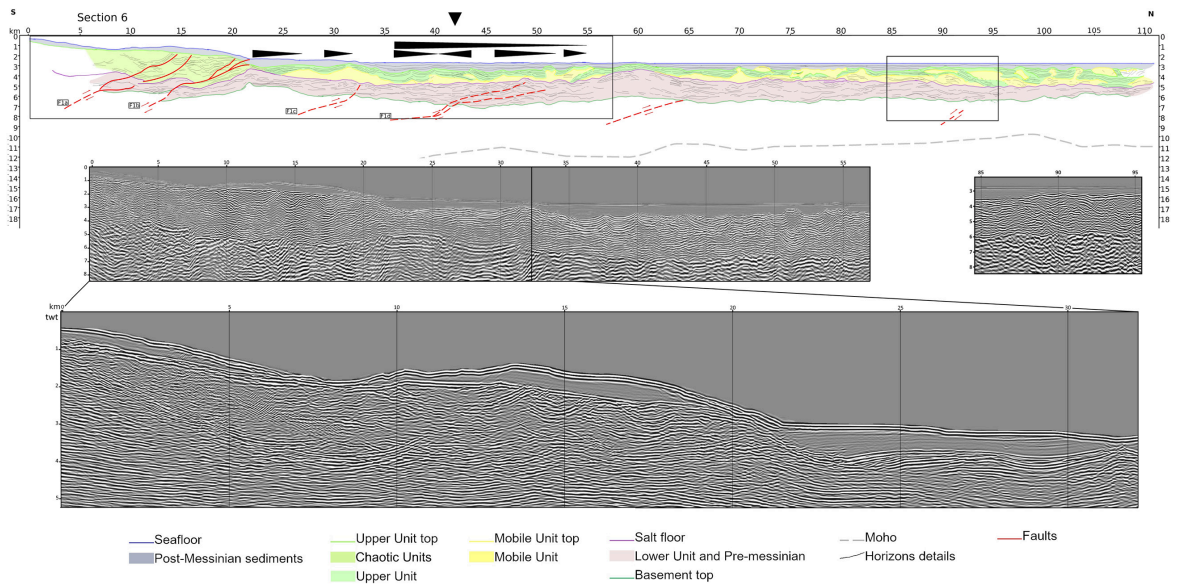

FIGURE 8 | Seismic Section 6 (Annaba) as a depth-converted line drawing. No vertical exaggeration. Major horizons and faults are identified, as well as major asymmetric basins. The insets display the raw depth-converted sections of the corresponding boxes. The inset on the second line is an extraction of the two-way-time section provided to better evidence faults-related shifts and the deformation of the sediments. Light green unit in the margin corresponds to the Messinian Complex unit (CU) coeval to UU and deposited in response to the major sea level drop of the Messinian Salinity Crisis. Stretched triangles: same as **Figure 6**. Downward pointing arrow locates the ocean-continent transition.

(Domzig et al., 2009; Medaouri et al., 2014; Badji et al., 2015; Soto et al., 2018), the tectonic inversion in the western zone appears to be limited in terms of faulting and flexure, but is expressed mostly by short wavelength undulations of the basement and strong Messinian salt halokinesis.

Central Zone (Tipaza to Bejaia Regions)

Location and Overall Structure

The central zone, located between Ténès and Bejaia (**Figure 2**), is the largest one but with an heterogeneous seismic coverage: indeed, the eastern half benefits from a relatively tight array of seismic lines when the western half area of Tenes is mostly uncovered. Although east-west changes in geometry actually exist, the lack of resolution does not allow us to precisely characterize along-strike evolutions from the central-western to the central margins. Moreover, faults and faults relay seems rather continuous between the two areas, so that we have merged them into one single zone.

Here, the margin features an alternation of basins and uplifted blocks with active thrusts dipping toward the south in the lower margin (submarine part, **Figure 6**) and one backthrust of opposite dip in the upper margin on land (Strzerzynski et al., 2021). Several sub-basins are found at the margin toe with lengths ranging from 60 to 90 km and a variable width (**Figures 9**, **10**). Some basement highs are visible on the eastern side of the region, in relation with the Hannibal High (**Figure 11**; Mauffret et al., 2004; Aïdi et al., 2018).

The western part of this area (Section 2, **Figure 6**) depicts horizon depths similar in range to the western zone, but with a contrasted morphology (e.g., a major uplifted block in the upper margin, interpreted as a former tilted block of the stretched margin; Yelles et al., 2009; Leprêtre et al., 2013). Previous studies have also evidenced deformation in the bathymetry and the shallowest sedimentary layers in the deep domain, especially off the 2003 Boumerdès rupture zone (**Figure 2**; Déverchère et al., 2005; Strzerzynski et al., 2010; Babonneau et al., 2017). They have evidenced the growth of piggy-back basins, suggesting the presence of three to five south-dipping thrust faults in the continental slope and the deep basin.

Seismic Sections 2 and 3

Section 2 (**Figure 6**) is representative of uplifted blocks areas around Algiers and the Khayr-al-Din bank (**Figure 1**). At the margin toe, the sedimentary basin is 3.2 km deep. The basin itself has an average depth of 5.2 km, with variations of approximately 500 m from km-65 to the northern tip of the section with a wavelength of more than 15 km. We also observe it on the other seismic sections of the Khayr-al-Din bank but not on seismic sections available further to the east. The basement also displays a relative low of 1 km amplitude at km-65, but it appears to correspond chiefly to a thickening of LU. A basement high separates this basin from a second basin located at the margin toe and the ocean/continent transition. MU is thicker from km-95 to the end of the seismic section than closer to the margin. This change mostly explains the deepening of the UU top by 1 km toward the margin. Therefore, we conclude that no significant DCF can be observed off the Khayr-al-Din, but that periodic undulations are present in the basement and the LU.

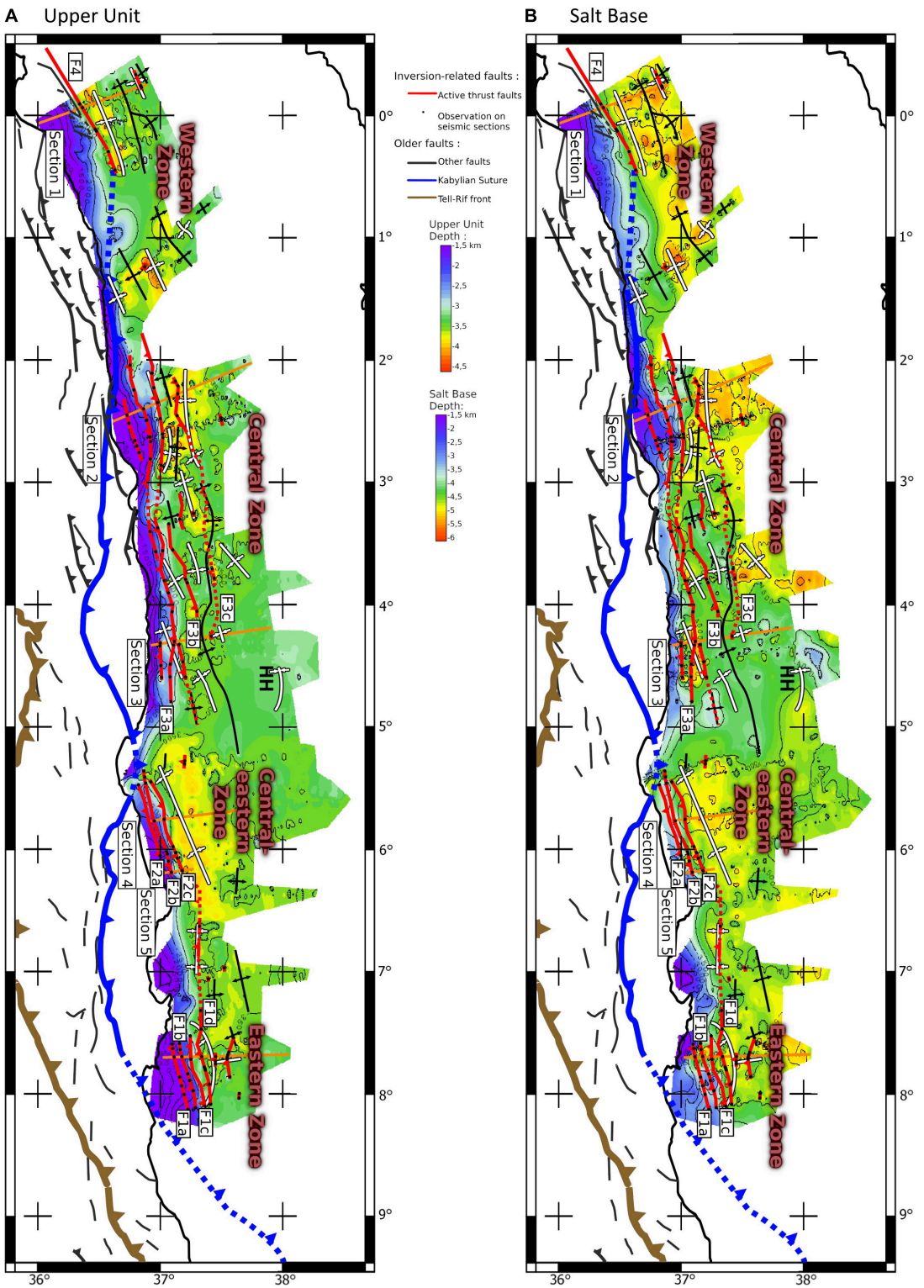

FIGURE 9 | Interpolated depth map of **(A)** upper unit top and **(B)** Mobile Unit base in the offshore domain. Main geological limits and active or inherited faults are plotted. Active thrust faults mapped here result from interpolation between the black dots which locate the direct or indirect imaging of faulting activity (close to the top of the basement) on seismic sections. In **(A,B)**, fault segments with the highest density of black dots are considered as the most reliable and are shown as continuous lines, while other segments are interpolated on longer distances and are shown as dotted curves (see text for details). HH marks the position of the Hannibal High.

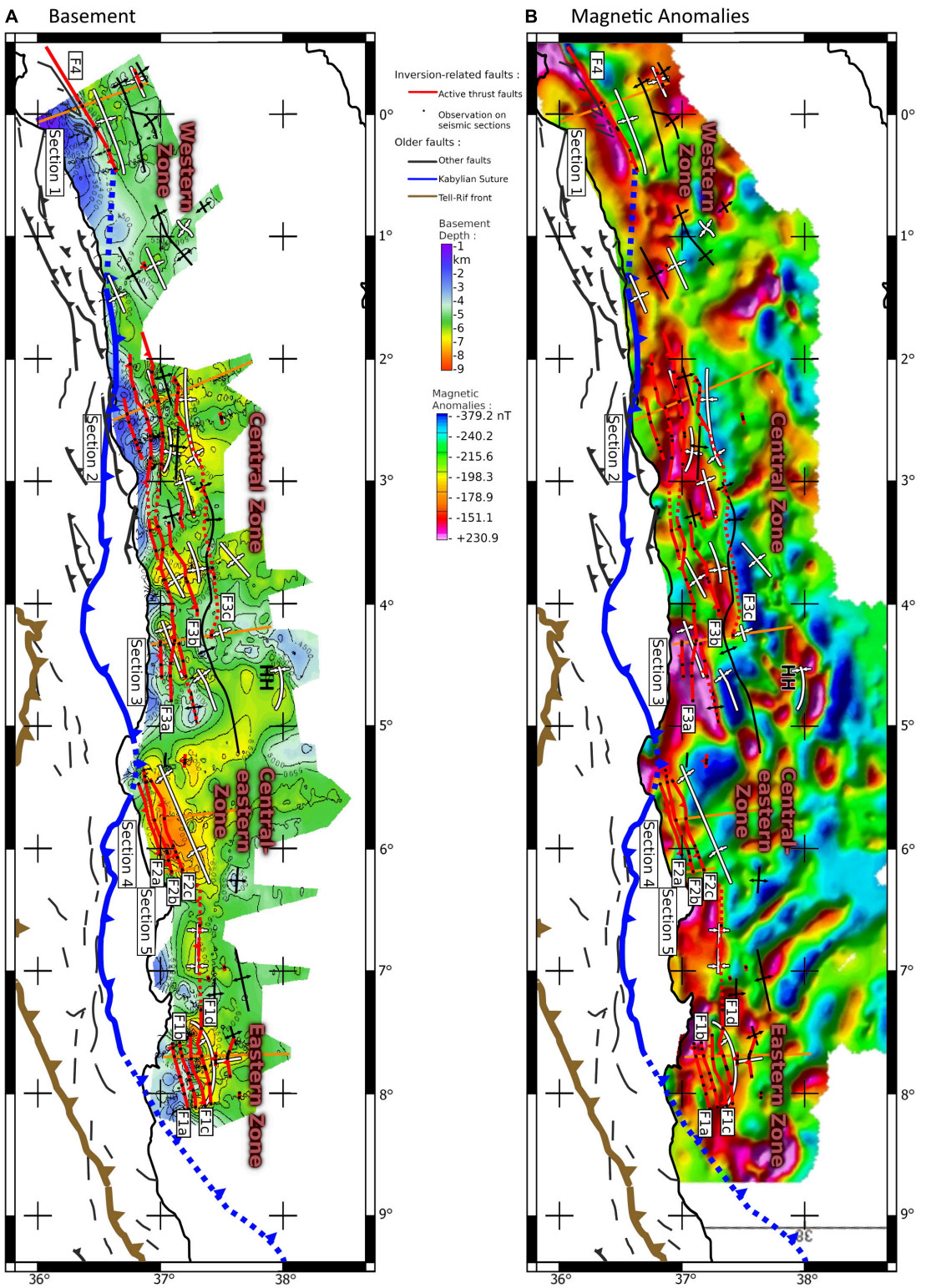

FIGURE 10 | Interpolated depth map of acoustic basement in the offshore domain **(A)**. Main geological limits and active or inherited faults are plotted. Active thrust faults mapped here result from interpolation between the black dots which locate the direct or indirect imaging of faulting activity (close to the top of the basement) on seismic sections. For comparison, **(B)** displays offshore reduced-to-the-pole magnetic anomalies (Medaouri, 2014) superimposed with the same structural sketch as above. HH marks the position of the Hannibal High. In **(A,B)**, fault segments with the highest density of black dots are considered as the most reliable and are shown as continuous lines, while other segments are interpolated on longer distances and are shown as dotted curves (see text for details).

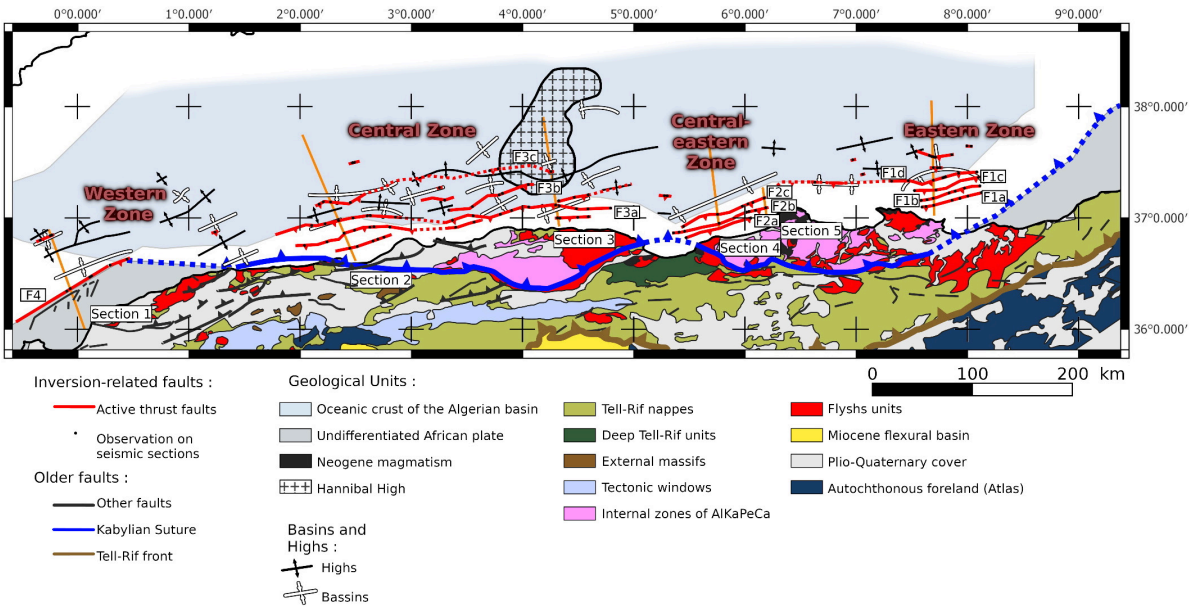

FIGURE 11 | Synthetic structural sketch of the Algerian margin displaying adjustments to already published fault systems based on the present work. Fault F4 is only partly shown on this map.

Regarding faults, the central-western area features a segmented basement structure, with 4 faults related to the inversion visible at basement top (**Figure 6**):

(1) The first fault (F3a upper branch) is observed near the top of the continental slope, around km-12.5, corresponding to a change in seafloor slope, a deformation of the sedimentary cover and a slope change of the basement top.
(2) The second fault (F3a lower branch), around km-34, is associated with a major uplift of the basement top. The sedimentary cover is also deeply disturbed, even if the imprint of the fault itself is not clearly identified. It seems also to correspond to a gentle decrease of the slope by 1 km over 5 km.
(3) The third fault at km-45 is the least well imaged on this section, associated with perturbations in the deepest sediments and in basement reflectors. They evidence an alignment that root at the same depth as similar faults in the area.
(4) The fourth fault at km-60 (F3c) is poorly imaged but clearly related to growth strata and folds in the sedimentary units without reaching the seafloor.

As a whole, the dip of these faults decreases toward the basin, from 25° to only 6° and they appear to control at least partly the morphology of the margin. Indeed, they locate in the steepest part of the margin but also create an asymmetric basin between km-23 and km-34 (Section 2. **Figure 6**), at a depth of around 3.2 km. Pre-Messinian to post-Messinian sedimentary units above are also folded. The basin itself might predate the inversion, being related to the opening of the Algerian basin. Discordances in the Messinian units reflect the uplift of the northern edge of the basin where more recent sediments are also uplifted up to the seafloor.

On Section 3 (**Figure 6**), in the basin, the basement gently declines by 1.6 km toward the margin from the end of the section to km-63. The basement is also characterized by a 40 km wide flat surface located between km-35 and km-55. Since pre-Messinian sediments are onlapping the basement, we consider this flat to be an inherited structure and not the signature of a DCF. The top of UU displays a progressive downward bending of 500 m amplitude toward the margin, while the basement displays a sharp deepening between km-35 and km-12.

Three main faults are identified along the continental slope:

(1) At km-5, the first fault (F3a) is imaged in the pre-Messinian sediments and is located right at the tip of a flat surface in the continental slope.
(2) The second fault (around km-12) identified in the basement also belongs to the F3a fault system and has a dip of 29°. The fault is associated with an important thickening of the sedimentary layer (up to 5 km) starting from km-23 and creating a perched basin in the lower part of the continental slope. These sediments are deformed both by secondary faults and by folding. The Lower Messinian and the basement also show a thickening caused at least partly by the fault activity and the associated folding. The seafloor in the projected continuity of the fault shows a gentle slope change separating the basin to the south from a flat in the continental slope at km-23.
(3) The last fault (F3c) splits into multiple branches upward. This fault shows a dip of 19° over its shallowest part but is unconstrained deeper in the basement. It correlates with tenuous shifts in the basement, in the sediments, and at

the foot of the continental slope, which could either be a coincidence, or the sign that the position of this continental slope is controlled by the recent tectonic activity of the Algerian margin.

Another fault (named F3b on **Figure 11**) is identified laterally between F3a and F3c but is not observed on the two sections displayed here. This fault reaches the basement and has a position similar to the northern branch of F3a on Section 3.

While Section 2 and 3 display rather different whole structures, major faulting at the basement top remains fairly similar, with a first fault situated high on the margin, a second major fault creating a flat in the continental slope, with or without uplifted block, and a third fault at the toe of the continental slope with basement deformation. Although we would need a tight seismic line coverage to better define the organization of uplifted blocks, these similarities in the faults structure between the two sections are considered to define the style of the central margin.

Interpolated Maps

The central margin features an east-west succession of 5 separated basins with lengths ranging between 40 and 55 km (**Figures 9**, **10**). Interpolated maps evidence the presence of the Hannibal High (**Figure 11**; Mauffret et al., 2004; Aïdi et al., 2018) in the eastern part of the area. The exact structure of the basin remains unclear because of a lack of sections imaging far enough into the basin, but we still evidence the flexure of the margin in the central part (**Figure 6**, section 3) with the depth of the basement varying from 6–7 km to 8–9 km. Strikes of the magnetic anomalies coincide quite well with the fault strikes (**Figure 10A**).

Central-Eastern Zone (Jijel)

Location and Overall Structure

The central-east zone is located offshore Jijel (**Figure 2**) and is characterized by a roughly similar structure across all seismic sections, suggesting the continuity of a sedimentary basin at the margin toe, with a length of at least 170 km and a width of 40 km (**Figure 9**), extending from the foot of the continental slope to the previously identified ocean-continent transition zone (Mihoubi et al., 2014). Here the half-wavelength of the DCF is between 150 and 170 km for an amplitude of 2 km at the top of the basement.

Seismic Sections 4 and 5

The structure of the basin along the Central-eastern margin displays a clear DCF of both the basement and the top of UU. Along Seismic Section 4 (**Figure 7**), the basement depths increase by 2 km over 160 km (only the first half of the section is shown in **Figure 7**, Seismic Section 4). Deepest reflectors in the basin corresponding to late Oligocene to Langhian deposits (Arab, 2016) are onlapping the basement and are related to the early filling after the formation of the margin. These onlapping sediments are about 1 km thick, not filling the whole DCF. Measurement at the salt base suggests a flexure less than one kilometer over the 160 km long Seismic Section 4 (**Figure 7**) where the UU thickness reaches 500 m. LU sediments are not onlapping the basement, therefore the DCF in this part of the margin necessarily post-dates the beginning of the Messinian salinity crisis.

This DCF is not accompanied by folding. Section 4 (**Figure 7**) is long enough to characterize the flexure, but is not extending far enough toward the margin and is too low in resolution to precisely image the margin faults. In order to better describe the margin and related faults, we rely on the depth-converted industrial Seismic Section 5 (**Figure 7**). We identify three main faults:

(1) Fault 1 (F2a on **Figure 11**), located on the highest part of the margin (km-14), is associated with both a smooth shift of the bathymetry and a deformation in the sedimentary cover. No basement shift is imaged on Section 5, but the strong deformation and the geometry of the fault suggest that it might be closely possible.
(2) Fault 2 (F2b on **Figure 11**) cuts through the basement around 5 km distance and reaches the UU in two branches between km-17 and km-20. As shown by the two-way traveltime inset (**Figure 8**), the basement depth varies over a short distance, which could indicate a shift by the fault. We also evidence small scarps (less than to 200 m high) in the bathymetry above these fault branches.
(3) Fault 3 (F2c on **Figure 11**) is located at the margin toe, reaching the basement around km-13.5 and cutting through the mobile unit at km-30. Here, we evidence a clear offset in the basement, characterized by the tiny overlap of the basement over the sedimentary cover. This overlap is at least 1.4 km long and implies a vertical displacement of ca. 1 km. The dip of this fault is estimated to be around 20° northward (ramp) and flattens toward the south in the mid pre-Messinian sedimentary cover, inducing some deformation in the horizons of the basin beyond the margin toe and between the salt.

It is worth noting that two more faults (identified as disconnected faults on Seismic Section 5, **Figure 7**) are located northward in relation with the second and third diapirs. They seem to die out at a depth close to the level where the third fault is flattening. This suggests that the deformation induced by Fault F2c propagates further into the basin, from 20 to 40 km at least, supporting thin-skin tectonics crossing through LU and MU.

Interpolated Maps

Magnetic anomalies of the eastern Algerian basin are oriented NW-SE to N-S and are related to the opening of this oceanic basin (Bayer et al., 1973; Cohen, 1980). In the deep basin and at the margin toe, several buried structures of the basement are related to magmatic events that affected the domain at ca. 17 Ma (Arab et al., 2016a,b; Abbassene et al., 2016; Chazot et al., 2017). A large, deep and asymmetric basin is superimposed to these structures but does not correlate with them. From its shape and position just north of the thrusts at the margin toe and at the continent-ocean transition, we infer that it is a large flexural basin that indicates a significant DCF that extends up to the Hannibal High westward. The southern limit of the basin also matches free air gravity anomalies of −70 to −80 mgal at the bottom of the continental slope (Mihoubi, 2014).

Eastern Zone (Annaba)

Location and Overall Structure

The eastern zone corresponds to the sector of Annaba (**Figure 2**) that presents a complex pattern, including several sub-basins apparently correlated to magnetic anomalies (**Figures 9**, **10**). The whole basin has a length of 90 km and a width of 25 km to 30 km, located between the ocean-continent transition to the north-west and the continental slope to the south (**Figure 8**, Section 6).

Seismic Section 6

The foot of the margin is marked by a basement high between km-20 and km-28, separating the margin from the basin, that might be related either to fault activity or to an inherited structure. The opposite end of Section 6 (**Figure 8**) to the north reveals a deepening of the salt base, a thickening of MU and intense salt tectonics that may support the presence of a fault around km-95. Without any other seismic section from our dataset extending far enough in the basin to image this area, we cannot further strengthen these hypotheses.

In the basin, the basement depth increases by 1.5 km over a distance of 60 km, from the north to the base of the continental slope, which gives a minimal amplitude and half-wavelength of the DCF in the eastern zone. The top of the basement is marked by at least three undulations, from km-0 to km-22.5 (including the basement high), from km-22.5 to km-48 and from km-48 to at least the end of the seismic section, which might reflect a crustal folding. Such folding is also evidenced on neighboring seismic sections. It appears consistent with the magnetic anomalies that show an east-west pattern. Actually, highs and lows in the basement of the basin correspond respectively to higher (–190 to –150 nT) and lower (–230 to –190 nT) values of the magnetic anomalies. Highs are proposed to be related to magmatism (Bouyahiaoui et al., 2015; Arab et al., 2016b) that could result from the Tethyan slab break-off, similarly to the Collo massif on land (Abbassene et al., 2016; Chazot et al., 2017). Basement faults in the basin also seem to be correlated with transitions from positive to negative magnetic anomalies.

Sedimentary deposits do not follow these variations. The very disrupted salt top (halokinesis) globally deepens by only 500 m (**Figure 8**) even if the volcanic edifice previously identified in the basin (Bouyahiaoui, 2014) (km-60 in **Figure 8**) locally interrupts this layer. This edifice is not covered by the MU but only by 500 m of UU sediments that are located above the UU layers in the surrounding area. The seafloor is also perturbed. These observations lead us to suggest that this ancient volcanic edifice is presently affected by an uplift, perhaps in relation with a fault proposed to be identified at km-65 on Section 6 (**Figure 8**) and also described on numerous adjacent sections.

The pre-Messinian and LU units are thickening toward the margin, inducing an uplift of the base of MU of 200–400 m on average. The presence of an asymmetric Plio-Quaternary basin and of a ramp of UU embedded in MU, correlated with deformations in earlier deposits, suggests the existence of a (not imaged) additional fault in the basin, probably around km-42. Southward, this part of the seismic section corresponds to a basement slope break at km-35, which is also located just underneath the base of the continental slope. It is worth noting that these two hypothesized faults are proposed to be localized at the inflection points of the basement undulations previously evidenced.

South of this high and below the slope, the basin displays a massive thickening, with up to 3 km of sediments assumed to represent (at least partly) Messinian Complex units (CU). This unit is affected by three faults (**Figure 8**) that merge into two when approaching the basement top. One of them (F1b on **Figure 11**) reaches the basement at km-13 and the two other ones (F1a) might reach it at km-7. While Fault 1 does not disturb post-Messinian sediments, suggesting that it does not participate in the accommodation of the convergence today, Fault 2 remains active up to the most recent sedimentary layers.

A third fault (F1c) is identified at km-33. Although it is not clearly imaged, it is inferred thanks to: (1) a step in the basement, (2) perturbations and folding in the lower sedimentary unit, (3) diapirism in MU and (4) deformation of the shallowest sediments (Quaternary) and the seafloor. This fault could explain, at least partly, the basement high previously described between km-20 and km-28 on Section 6. Such a blind thrust fault system has also been described on higher resolution MARADJA seismic lines from this same area of the Algerian margin (Kherroubi et al., 2009). A last thrust (F1d) is assumed further north (**Figure 8**).

Faults along the eastern margin are not well constrained in the basement, but we can propose estimated dip values from our sections. They are around 27° for the first two upper faults of the continental slope (F1a and F1b), responsible for most of the deformation in the sedimentary layers, and respectively 14° and 6° for the two other ones in the basin (F1c and F1d).

Interpolated Maps

On the interpolated maps, we evidence a DCF in the monitored horizons, especially the basement (**Figure 10**) where it is not perturbed by the presence of the volcanic edifice, concentrated on the northern part of the eastern zone. The shape of the sedimentary layers support a tectonic thickening of the sedimentary cover by wedging (visible south of km-22 on Section 6). The flexural basin is imaged north of this thickened region, hence covering only the northern half of the section. The basin at the toe of the continental slope is correlated to magnetic anomalies, but also to gravimetric anomalies (Bouyahiaoui, 2014) which present a negative value from –51.3 to –40 up north of the continental slope.

DISCUSSION

We have attempted to gather markers of ongoing deformation of the deep Algerian basin undergoing tectonic shortening. We have identified three modes of basin deformation expected to be a "standard" response of the lithosphere to compression but are sometimes overlooked (Cloetingh et al., 1999; Burov, 2011; Cloetingh and Burov, 2011): (1) a downward bending of the oceanic-type lithosphere at the margin toe, hereafter called downward concave flexure (DCF); (2) a buckling (folding) of the oceanic lithosphere expressed by crustal undulations

perpendicular to the direction of compression, and (3) a localized deformation at the margin toe revealing underthrusting of the oceanic lithosphere. We summarize hereafter the characteristics and relationships of these modes of active deformation. Regarding the age of the faulting, we have no way to discuss it with our data set owing to the poor resolution of the seismic data. Nevertheless, from our observations on all the seismic lines (fault shifts and wedge-shaped basins, **Figures 3**, **5–8**), it appears that fault activity mostly post-dates Messinian deposits, as generally inferred in the offshore domain of Algeria (see a full discussion in this respect in Strzerzynski et al., 2021).

Downward Concave Flexure of the Oceanic Lithosphere

The strong asymmetry of the Plio-Quaternary basins off Algeria, coincident to a significant negative gravity anomaly, was used by Auzende et al. (1975) to suggest an early stage of active margin evolution. The mapping of three major seismic horizons (upper unit top, Mobile Unit base and acoustic basement, **Figures 9A,B**, **10A**, respectively) indeed reveals a significant permanent deformation. This deformation is proposed to result from a downward concave flexure (DCF) of the oceanic lithosphere. Its general orientation (i.e., roughly perpendicular to the maximum stress direction of relative convergence between the African and Eurasian plates) and the amplitude and wavelength of the DCF are quite consistent with models derived from gravity anomalies (Hamai et al., 2015). What is striking is the discontinuous pattern of these DCF anomalies recorded simultaneously on the 3 seismic horizons, which also coincides with the pattern of the thrust faults (**Figures 9**, **10**). The first order match between the models derived from the gravimetry and the DCF maps and the overall concave shape and asymmetry of these horizons are strong arguments to consider this interpretation as robust enough, in spite of the uncertainties regarding the time-to-depth conversion and gaps in the seismic network used.

Table 2 shows that the DCF has a greater half-wavelength (ca. 160 km) and amplitude (ca. 2 km) in the central-eastern segment (Jijel) than in the other areas. This area would then be prone to load a significant amount of elastic strain that could result in a strong magnitude earthquake. This area indeed bore the 1856 Jijel earthquake, which is among the strongest events ever felt along the Algerian coast and was followed by a tsunami (Boughacha et al., 2004; Yelles-Chaouche et al., 2009). The easternmost basin (Annaba) also displays a similar DCF pattern (**Figures 9**, **10**) with an amplitude of 1.5 km but over a much shorter distance of 60 km. The third area submitted to a relatively significant flexural loading (i.e., 77 km half-wavelength and 0.5 km amplitude, **Table 2**) is the central/central-western zone (**Figures 9**, **10**), off the cities of Tipaza, Algiers and Boumerdès, where several historical and instrumental seismic events occurred (Ayadi et al., 2003; Boughacha et al., 2004). Finally the westernmost area (Oran-Mostaganem) as well as the central-western (Algiers) does not evidence any significant flexural loading, suggesting that these two areas are not prone to significant seismic loading.

Buckling of the Oceanic Lithosphere

Short wavelength undulations of the seismic horizons sub-parallel to the Algerian margin are evidenced in the oceanic domain of the western zone (section 1), the western part of the central zone (section 2) and the eastern zone (section 6) (**Figures 9–11** and **Table 2**), with a mean wavelength of 30–35 km and an amplitude of about 800–1000 m. This oscillant pattern is particularly well expressed just north-west of the linear and narrow margin of Mostaganem (Domzig et al., 2009; Badji et al., 2015) and a bit less north of the Khayr-Al-Din bank (**Figure 1**), whereas it appears more questionable in the easternmost margin where the top of the basement is affected by Miocene volcanics (Bouyahiaoui et al., 2015). As predicted by folding theory and simulations, the anticlines display lower amplitudes than synclines as a result of the contribution of gravity (Cloetingh et al., 1999; Cloetingh and Burov, 2011).

For the western and central-western zones, we hypothesize that this pattern reveals a buckling of the oceanic lithosphere with fold axes perpendicular to the relative plate convergence, with a dominant control of the brittle crust (Burov, 2011). We suggest that this buckling is mostly due to a combination of two parameters: (1) the narrowness of the oceanic basin west of Algiers, which may explain why the brittle layer cannot bend over a long distance, and (2) the presence of a STEP-fault margin that acts as a buttress, preventing strain focusing at the margin toe and thus transferring compression further north toward the Betic margin (Giaconia et al., 2015) or further south on the Algerian coast (Yelles-Chaouche et al., 2006). A similar buckling of the East Japan basin floor (combined with limited underthrusting) is reported along the eastern Korean wrench margin (Kim et al., 2018), but with a longer wavelength (60–70 km) and smaller amplitude (200 m).

It is also worth noting that if we assume a wavelength of folding of approximately seven times the brittle layer thickness (Bull et al., 1992), the latter would be of about 4–5 km in the western Algerian basin, a value which is close to the mean thickness of the oceanic crust identified in the wide-angle experiments off Mostaganem and Tipaza, i.e., 3–4 km in Badji et al. (2015) and 5–6 km in Leprêtre et al. (2013), respectively. This ratio is also true in the case of the East Japan sea, where the crustal thickness is ∼11 km (Kim et al., 2018).

For the eastern zone, the structures of the crust evidenced by the magnetic anomalies could act as focal points for the deformation, forcing the eventual buckling to overprint itself over them.

Active Fault Network and Tectonic Style of the Algerian Margin

Our analysis provides for the first time a comprehensive and coherent overview of the main deep active faults of the Algerian margin. The fault mapping offshore was until now the object of quite conflicting representations. We report for instance the large differences between interpretations by Mauffret (2007); Meghraoui and Pondrelli (2012), and Rabaute and Chamot-Rooke (2015). The interpretation we propose here results from a full revision of all data available and gather the deepest

information in order to avoid the mapping of subsurface faults that may appear as secondary faults systems driven by the formation of rollovers or by Messinian salt halokinesis and gravity gliding or spreading (e.g., Déverchère et al., 2005; Gaullier et al., 2006; Domzig et al., 2009; Kherroubi et al., 2009; Cattaneo et al., 2010; Strzerzynski et al., 2010; Arab et al., 2016b). Among striking differences, our structural sketch (**Figure 11**) clearly differs from the one by Mauffret (2007) who hypothesized a single, continuous fault running from the easternmost margin to Greater Kabylia and a left-lateral wrench fault in the western margin (Arzew escarpment). Our result also invalidates the model of restraining bend by Meghraoui and Pondrelli (2012) featuring a ∼350 km long right-lateral fault striking West-East at the margin toe between the bay of Bejaia and the Khayr-Al-Din bank. It also shows that the active faults in the basement at depth are likely more continuous than fault segments mapped from subsurface data (Kherroubi et al., 2009; Rabaute and Chamot-Rooke, 2015; Kherroubi et al., 2017).

Several studies have also proposed through seismic reflection data acquisition or experimental modeling that the Algerian margin is deforming by crustal flat-ramp systems (Déverchère et al., 2005; Roure et al., 2012; Aïdi et al., 2018; Strzerzynski et al., 2021), implying a crustal decoupling layer in the lower crust of the stretched continental margin (Kherroubi et al., 2017). However, whether this mixed thin-skinned and thick-skinned tectonic style is the rule over the whole margin segments is unclear. Our study suggests that outward propagation of the faulted systems driven by thick-skinned thrusts is actually taking place only in the central zone (**Figure 11**), i.e., the Greater Kabylian block, sometimes called the "Maghrebian indenter" (Piqué et al., 1998), as this is the only area where we observe faults in the oceanic basement unrelated to buckling, whereas very limited propagation by decollements is occurring in the central-eastern and eastern zones, and no propagation in the western zone (**Figure 11**). This result suggests that the position of the indenter of the central zone may play a significant role in its relative maturity compared to the other segments and likely reflects an important inherited effect of the phase of opening of the Algerian domain (van Hinsbergen et al., 2014, 2020 and references therein).

Possible Implications for Seismic Hazards Off Algeria

Our study offers the opportunity to assess more realistic estimates of maximum magnitude of earthquakes off Algeria owing to a systematic examination of active faults rooted in the basement, where large earthquakes are assumed to nucleate. Here, we propose to rely on our interpretations and lateral correlation hypothesized from our seismic sections across the Algerian margin to compute a range of maximum magnitudes (**Table 3**) and to discuss briefly their consistency with historical and instrumental seismicity.

Relationships between the length of a rupture and the magnitude of an earthquake have been discussed since long (e.g., Wells and Coppersmith, 1994; Stirling et al., 2013, and references therein). Here, we use the regression equations summarized by Stirling et al. (2013) for reverse faults and for magnitude ranging from 6.1 to 9.5 to propose possible magnitude ranges (**Table 3**).

The western area (**Figure 11**) features a unique fault (F4) of ca. 180 km (Domzig et al., 2009; Badji et al., 2015), equivalent to a magnitude 7.6. However, this fault does not affect significantly the most recent layers at the margin toe (Domzig et al., 2009). Considering: (1) the STEP-fault related sub-vertical geometry of the margin (Govers and Wortel, 2005; Badji et al., 2015), (2) its strike orthogonal to the direction of convergence, (3) the very limited underthrusting at depth (Medaouri et al., 2014) and (4) the lack of significant flexural loading (see section "Downward Concave Flexure of the Oceanic Lithosphere"), we suggest that this segment is barely active and does not produce large earthquakes, although exceptional ruptures cannot be discarded. This interpretation agrees with the absence of major seismic events in the area, except the 1790 event which source is assumed to be related to faults located westward (Buforn et al., 2019).

In the central area, several short fault segments are reported close to the coastline, which are proved to produce moderate-size events of magnitude 6.0–6.5, like for instance the 1989 earthquake (Meghraoui, 1991). If we consider only the longer faults of our structural sketch, we identify segments of lengths reaching typically 60-70 km (for instance Fault F3b, Section 3), as the one which led to the dramatic M 6.9 2003 Boumerdes-Zemmouri earthquake (Ayadi et al., 2003), with cumulative fault scarps close to the margin toe (Déverchère et al., 2010; Kherroubi et al., 2017). The average spacing of these thrusts is between 5 and 15 km, which is typical of thin-skinned thrust belts (Morellato et al., 2003). This is also the typical magnitude expected from a rupture at the toe of the Khayr-Al-Din bank (Yelles et al., 2009). If we assume that the Boumerdes thrust fault to the East is linked at depth with the Khayr-Al-Din fault to the west, we obtain a total length of ca. 280 to 310 km (Fault F3a), equivalent to a magnitude 7.9–8.0. Finally, the northernmost thrust segment (F3c) reaches a length of ca. 240 km, but whether this thrust rooting on a decollement layer (Déverchère et al., 2005; Roure et al., 2012) may produce earthquakes separately from the other faults segments located within the margin further south (like the 2003 Boumerdes-Zemmouri event) and which are rooting on this same decollement layer is questionable. In this zone, recurrence intervals from paleoseismology range between 300 and 1600 years (Ratzov et al., 2015; Babonneau et al., 2017),

TABLE 3 | Lengths of faults estimated at the basement top according to the structural sketch of **Figure 11**, and estimated values of magnitudes using statistical relationships for thrust faults in Stirling et al. (2013).

Zone (Figure 1)	Fault number (Figure 11)	Estimated length (km)	Maximum magnitude
Western zone	F4	**180**	**7.6**
Central	F3c	**240**	**7.8**
	F3b	**70**	**7.0**
	F3a	**280–310**	**7.9–8.0**
Central-Eastern	F2a, b, c	**120**	**7.3**
Eastern	F1a, b, c, d	**60**	**6.9**
Central-Eastern and Eastern (merged)	F1d + F2c	**310**	**8.0**

therefore suggesting irregular earthquake cycling but relatively frequent earthquake occurrences.

In the central-eastern area, a typical fault length of 120 km is found at the margin toe (F2a, F2b, F2c) on sub-parallel segments with a close spacing of 5–10 km. If we assume that these segments root in the same deep segments, as proposed by Arab et al. (2016b), this would imply earthquakes with a magnitude of 7.4, a magnitude which has been typically assumed for the 1856 Jijel earthquake (Boughacha et al., 2004; Yelles-Chaouche et al., 2009).

Finally, the eastern margin displays close thrust segments (F1a, F1b, F1c, F1d) with typical lengths of ∼60 km, implying events of magnitude less than 7 (**Table 3**). They are likely rooting on a single deep fault, as suggested by their close spacing and the deep seismic experiments (Bouyahiaoui et al., 2015). If we hypothesize that faults F1d may be activated together with segment F2c in a single event (which is not excluded according to our mapping in **Figure 11**), this would lead to a maximum length of ∼310 km and a magnitude 8.0 event. However, historical seismicity did nor reveal any significant strong event in the eastern zone (Kherroubi et al., 2009), thus it remains difficult to conclude on the occurrence of such a large magnitude event. Recurrence intervals from paleoseismology have not been yet documented in this zone, but if we follow the GPS velocity model by Bougrine et al. (2019), strain rates offshore are likely 2 or 3 times less than in the central zone, therefore historical seismicity cannot be considered as sufficient to discard the occurrence of such earthquakes in the future.

CONCLUDING REMARKS

North Africa accommodates the convergence of Eurasian and African plates since Late Cretaceous times. Since the closure of the Tethyan oceanic lithosphere and the docking of the Kabylian blocks with Africa ∼19 Myr ago, the transpression induced by the relative plate convergence has been likely accommodated by a combination of shortening along large thrust fault systems onland and clockwise block rotations (book-shelf faulting) in the Tell-Atlas fold-and-thrust belts (Frizon de Lamotte et al., 2000, 2009; Roure et al., 2012; Derder et al., 2019). The relative importance of each process has long been debated (e.g., Frizon de Lamotte, 2005). However, the way convergence is absorbed likely evolves through times. Both our study of strain markers in the offshore domain and recent results of active strain distribution on land (Bougrine et al., 2019) support that northern Algeria is witnessing the birth of a new plate boundary since Plio-Quaternary times, at the place where the back-arc extensional and wrench systems of the western Mediterranean Sea are undergoing a tectonic inversion potentially preceding a subduction. Three main systems are identified:

(1) In the western zone (Mostaganem segment, **Figure 11**), the inherited transform-type (STEP) margin acts as a long-term locked, stiff limit where strain is transferred toward the north by buckling of the young oceanic lithosphere and thrusting of opposite vergence in the neighboring continental margins of Iberia and Africa. Although a magnitude 7 event on this offshore structure cannot be ruled out, we speculate that strain accumulation occurs only at very slow rates.

(2) In the central zone of Algeria (Tipaza-Greater Kabylia segment, **Figure 11**), we evidence an oceanward propagation of north-verging thrust ramps rooting on thin-skinned detachments and on a thick-skinned thrust systems in the continental margin, together with a mixture of moderate downward concave flexure and buckling of the oceanic lithosphere. This tectonic style is typical of foreland fold-and-thrust belts (e.g., Frizon de Lamotte et al., 2000, 2009; Garcia-Castellanos and Cloetingh, 2012; Roure et al., 2012; Alania et al., 2017) and agrees with a model where active deformation is dominantly accommodated by internal deformation of the oceanic domain and by thrust faults striking almost perpendicular to the relative plate convergence, without the need for significant right-lateral strike-slip faulting (Bougrine et al., 2019). Fault continuity suggests ruptures around magnitude 7 (as exemplified by the 2003 Boumerdès-Zemmouri earthquake) but potentially up to magnitude 8 if rupture is inferred along the entire length of adjacent fault segments.

(3) In the central-eastern and eastern zones of Algeria (Lesser Kabylia segment, **Figure 11**), we evidence a long wavelength and high amplitude flexure of the oceanic lithosphere without significant buckling, together with a set of sub-parallel, closely spaced north-verging thrust ramps rooting in the basement of Lesser Kabylia without northward propagation in the oceanic domain. This tectonic style recalls splay fault systems evidenced in mature accretionary wedges of subduction (e.g., Park et al., 2002; Strasser et al., 2009), however the way the faults connect at greater depth below Lesser Kabylia is not imaged. In the eastern zone off Annaba, flexural bending is decreasing and fault segments are shorter. As no oblique or strike-slip faulting is evidenced offshore, our findings agree with a kinematic model where active strain is partitioned between right-lateral strike-slip motion on the Ghardimaou-North-Constantine (GNC) fault on land and reverse faulting offshore (Bougrine et al., 2019). Fault continuity suggests ruptures around magnitude 7.3–7.5 on the offshore thrusts, as recorded during the 1856 Jijel earthquake.

It remains now necessary to examine how the offshore, segmented active thrust faults described here connect to sub-parallel onland thrust faults like the Blida and Cheliff faults (Yelles-Chaouche et al., 2006). Although there is no evidence for simultaneous rupture across adjacent segments at sea and on land until now, the fault structural maturity (Manighetti et al., 2007) should be carefully examined in the future in order to better assess seismic hazards in Algeria.

Post-submission Addendum

On 18 March 2021 at 00:04 UTC, a Mw 6.0 earthquake occurred in northeastern Algeria in the Bay of Bejaia (**Figure 2**).

This event is located at the westernmost tip of the thrust fault labeled F2b in our study (**Figure 11**) and occurred after a succession of moderate magnitude thrust events near our mapped thrusts F2 in 2014–2019 (Yelles-Chaouche et al., 2021). We have identified Fault F2b as a blind reverse fault gently dipping southward (**Figure 7**), striking locally almost W-E and apparently merging at this place with Fault F2c (**Figures 10**, **11**). These faults are parts of a system of 3 sub-parallel thrusts that are assumed to represent the upper part of the active fault responsible for the magnitude 7.5 1856 Jijel earthquake (Yelles-Chaouche et al., 2009, 2017).

We have underlined the similarity of this thrust fault system with splay faults evidenced in mature accretionary wedges of subduction. Although we ignore how these faults connect at greater depth below Lesser Kabylia, we note that Fault F2b matches quite well the parameters of the March 2021 focal solution[1] regarding strike (almost E-W), type of faulting (pure reverse) and dip angle of the southern nodal plane ($25° \pm 10°$). This event could therefore be understood as expressing a process of static stress loading and stress transfer at the westernmost tip of the rupture zone of the 1856 Jijel earthquake, which is among the largest historical events identified off Algeria. This recent seismic activity off Jijel further supports that the F2 fault system is a major seismogenic structure representing the reverse component of a strain partitioning fault system (Bougrine et al., 2019; Yelles-Chaouche et al., 2021).

Finally, we believe that co-seismic rupture at the sea bottom linked to the 2021 Bejaia event is unlikely, provided that the expected coseismic slip for such a magnitude is very small and that the bay of Bejaia is occupied by a giant, active deep-sea fan (Cattaneo et al., 2010).

DATA AVAILABILITY STATEMENT

The data set analyzed in this study is subject to the following licenses/restrictions: Seismic data from the SPIRAL cruise (DOI 10.17600/9010050) are managed by SISMER (Ifremer) and are submitted to a restricted access, except MGD77 data. Additional industrial lines are provided by SONATRACH and are submitted to SPIRAL partnership agreement rules. Requests to access these data sets should be directed to MA, mohamed.arab@sonatrach.dz.

[1] https://www.emsc-csem.org/

AUTHOR CONTRIBUTIONS

PL interpreted and converted the seismic sections. JD supervised the steps of the research project. DG, FK, MA, and MM provided support in the research, data interpretation, and discussed the results. All authors participated in the writing and improvement of the manuscript.

FUNDING

We acknowledge Ph.D. scholarship funding from the French Government (PL) and support by the TelluS Program of CNRS/INSU (ALEAS call 2020, Project COTISIS).

ACKNOWLEDGMENTS

We would like to thank all the people involved in the SPIRAL project, from CRAAG (Centre de Recherche en Astronomie, Astrophysique et Géophysique), DGRST (Directorate-General for Scientific Research and Technological Development), CNRS (Centre National de la Recherche Scientifique), Ifremer (Institut Français de Recherche pour l'Exploitation de la Mer), IRD (Institut de Recherche pour le Développement), Universities of Brest and Nice, as well as Sonatrach (Société nationale pour la recherche, la production, le transport, la transformation, et la commercialisation des hydrocarbures). We also thank Juan I. Soto (University of Granada, Spain) for his help on improving the interpretation of the salt tectonics and Marie-Odile Beslier (CNRS, Géoazur Nice) for her useful advice on improvement to our interpretation. This work has used the Kingdom Suite seismic and geological interpretation software as well as QGIS software. The constructive reviews of the three reviewers are gratefully acknowledged.

REFERENCES

Abbassene, F., Chazot, G., Bellon, H., Bruguier, O., Ouabadi, A., Maury, R. C., et al. (2016). A 17 Ma onset for the post-collisional K-rich calc-alkaline magmatism in the Maghrebides: evidence from Bougaroun (northeastern Algeria) and geodynamic implications. *Tectonophysics* 674, 114–134. doi: 10.1016/j.tecto.2016.02.013

Aïdi, C., Beslier, M.-O., Yelles-Chaouche, A. K., Klingelhoefer, F., Bracene, R., Galve, A., et al. (2018). Deep structure of the continental margin and basin off Greater Kabylia, Algeria – New insights from wide-angle seismic data modeling and multichannel seismic interpretation. *Tectonophysics* 728–729, 1–22. doi: 10.1016/j.tecto.2018.01.007

Alania, V., Chabukiani, A., Chagelishvili, R., Enukidze, O., Gogrichiani, K., Razmadze, A., et al. (2017). Growth structures, piggy-back basins and growth strata of Georgian part of Kura foreland fold-thrust belt: implication for Late Alpine kinematic evolution. *Geol. Soc. Spec. Publ.* 428, 171–185. doi: 10.1144/SP428.5

Arab, M. (2016). *Analyse des systèmes pétroliers de l'offshore Algérien oriental: Quantification, modélisation stratigraphique et thermique.* Brest, Université de Bretagne Occidentale, 175.

Arab, M., Belhai, D., Granjeon, D., Roure, F., Arbeaumont, A., Rabineau, M., et al. (2016a). Coupling stratigraphic and petroleum system modeling tools in complex tectonic domains: case study in the North Algerian Offshore. *Arab. J. Geosci.* 9:289. doi: 10.1007/s12517-015-2296-3

Arab, M., Rabineau, M., Déverchère, J., Bracene, R., Belhai, D., Roure, F., et al. (2016b). Tectonostratigraphic evolution of the eastern Algerian margin and basin from seismic data and onshore-offshore correlation. *Mar. Pet. Geol.* 77, 1355–1375. doi: 10.1016/j.marpetgeo.2016.08.021

Authemayou, C., Pedoja, K., Heddar, A., Molliex, S., Boudiaf, A., Ghaleb, B., et al. (2017). Coastal uplift west of Algiers (Algeria): pre- and post-Messinian sequences of marine terraces and rasas and their associated drainage pattern. *Int. J. Earth Sci.* 106, 19–41. doi: 10.1007/s00531-016-1292-5

Auzende, J.-M., Bonnin, J., and Olivet, J.-L. (1975). La marge nord-africaine considérée comme marge active. *Bull. Soc. Géol. France* 7, 486–495. doi: 10.2113/gssgfbull.S7-XVII.4.486

Ayadi, A., Maouche, S., Harbi, A., Meghraoui, M., Beldjoudi, H., Oussadou, F., et al. (2003). Strong Algerian earthquake strikes near Capital city. *EOS* 84, 561–568. doi: 10.1029/2003eo500002

Babonneau, N., Cattaneo, A., Ratzov, G., Déverchère, J., Yelles-Chaouche, A. K., Lateb, T., et al. (2017). Turbidite chronostratigraphy off Algiers, central Algerian margin: a key for reconstructing Holocene paleo-earthquake cycles. *Mar. Geol.* 384, 63–80. doi: 10.1016/j.margeo.2016.10.017

Badji, R. (2014). *Structure profonde de la croûte et potentiel pétrolier des bassins Sédimentaires à l'ouest de l'Algérie*. Ph.D. thesis. Nice, Université Nice – Sophia Antipolis, 160.

Badji, R., Charvis, P., Bracene, R., Galve, A., Badsi, M., Ribodetti, A., et al. (2015). Geophysical evidence for a transform margin offshore Western Algeria: A witness of a subduction-transform edge propagator? *Geophys. J. Int.* 200, 1029–1045. doi: 10.1093/gji/ggu454

Bayer, R., Le Mouel, J. L., and Le Pichon, X. (1973). Magnetic anomaly pattern in the western mediterranean. *Earth Planet. Sci. Lett.* 19, 168–176. doi: 10.1016/0012-821X(73)90111-8

Billi, A., Faccenna, C., Bellier, O., Minelli, L., Neri, G., Piromallo, C., et al. (2011). Recent tectonic reorganization of the Nubia-Eurasia convergent boundary heading for the closure of the western Mediterranean. *Bull. Soc. Géol. France* 182, 279–303. doi: 10.2113/gssgfbull.182.4.279

Booth-Rea, G., Ranero, C. R., and Grevemeyer, I. (2018). The Alboran volcanic-arc modulated the Messinian faunal exchange and salinity crisis. *Sci. Rep.* 8:13015. doi: 10.1038/s41598-018-31307-7

Booth-Rea, G., Ranero, C. R., Martínez-Martínez, J. M., and Grevemeyer, I. (2007). Crustal types and Tertiary tectonic evolution of the Alborán sea, western Mediterranean. *Geochem. Geophys. Geosyst.* 8:Q10005. doi: 10.1029/2007GC001639

Boughacha, M. S., Ouyed, M., Ayadi, A., and Benhallou, H. (2004). Seismicity and seismic hazard mapping of northern Algeria: map of Maximum Calculated Intensities (MCI). *J. Seismol.* 8, 1–10. doi: 10.1023/B:JOSE.0000009513.11031.43

Bougrine, A., Yelles-Chaouche, A. K., and Calais, E. (2019). Active deformation in Algeria from continuous GPS measurements. *Geophys. J. Int.* 217, 572–588. doi: 10.1093/gji/ggz035

Bouillin, J.-P., Durand-Delga, M., and Olivier, Ph. (1986). Betic-rifian and tyrrhenian arcs: distinctive features, genesis and development stages. *Dev. Geotectonics* 21, 281–304. doi: 10.1016/B978-0-444-42688-8.50017-5

Bouyahiaoui, B. (2014). *Structure profonde et réactivation de la marge est-Algérienne et du bassin adjacent (secteur d'Annaba), contraintes par sismique-réflexion multitrace et grand-angle terre-mer*. Ph.D. thesis. Nice, Université Nice – Sophia Antipolis, 232.

Bouyahiaoui, B., Sage, F., Abtout, A., Klingelhoefer, F., Yelles-Chaouche, K., Schnürle, P., et al. (2015). Crustal structure of the eastern Algerian continental margin and adjacent deep basin: implications for late Cenozoic geodynamic evolution of the western Mediterranean. *Geophys. J. Int.* 201, 1912–1938. doi: 10.1093/gji/ggv102

Brewer, J. (1987). *Seismic Reflection Studies of Major Crustal Faults. In: Structural Geology and Tectonics. Encyclopedia of Earth Science*. Berlin: Springer. doi: 10.1007/3-540-31080-0_97

Brun, J. P., and Fort, X. (2011). Salt tectonics at passive margins: geology versus models. *Mar. Pet. Geol.* 28, 1123–1145. doi: 10.1016/j.marpetgeo.2011.03.004

Buforn, E., Coca, P., Bezzeghoud, M., Udías, A., Bouhadad, Y., and Mattesini, M. (2019). The destructive 1790 Oran (NW Algeria) earthquake in a region of low seismicity. *Tectonophysics* 759, 1–14. doi: 10.1016/j.tecto.2019.03.008

Bull, J. M., Martinod, J., and Davy, P. (1992). Buckling of the oceanic lithosphere from geophysical data and experiments. *Tectonics* 11, 537–548. doi: 10.1029/91TC02908

Burov, E. B. (2011). Rheology and strength of the lithosphere. *Mar. Pet. Geol.* 28, 1402–1443. doi: 10.1016/j.marpetgeo.2011.05.008

Burov, E. B., and Diament, M. (1995). The effective elastic thickness (Te) of continental lithosphere: What does it really mean? *J. Geophys. Res. Solid Earth* 100, 3895–3904. doi: 10.1029/94JB02770

Calvert, A. J. (2004). A method for avoiding artifacts in the migration of deep seismic reflection data. *Tectonophysics* 388, 201–212. doi: 10.1016/j.tecto.2004.07.026

Calvert, A. J. (2017). Continuous estimation of 3-D reflector orientations along 2-D deep seismic reflection profiles. *Tectonophysics* 718, 61–71. doi: 10.1016/j.tecto.2016.11.002

Camerlenghi, A., Accettella, D., Costa, S., Lastras, G., Acosta, J., Canals, M., et al. (2009). Morphogenesis of the SW Balearic continental slope and adjacent abyssal plain, Western Mediterranean Sea. *Int. J. Earth Sci.* 98, 735–750. doi: 10.1007/s00531-008-0354-8

Cattaneo, A., Babonneau, N., Dan, G., Déverchère, J., Domzig, A., Gaullier, V., et al. (2010). "Submarine landslides along the Algerian margin: a review of their occurrence and potential link with tectonic structures," in *Submarine Mass Movements and Their Consequences. Advances in Natural and Technological Hazards Research*, Vol. 28, eds Mosher D.C. et al. (Dordrecht: Springer). doi: 10.1007/978-90-481-3071-9_42

Chazot, G., Abbassene, F., Maury, R. C., Déverchère, J., Bellon, H., Ouabadi, A., et al. (2017). An overview on the origin of post-collisional Miocene magmatism in the Kabylies (northern Algeria): evidence for crustal stacking, delamination and slab detachment. *J. Afr. Earth Sci.* 125, 27–41. doi: 10.1016/j.jafrearsci.2016.10.005

Cloetingh, S., Burov, E., and Poliakov, A. (1999). Lithosphere folding: Primary response to compression? (from central Asia to Paris basin). *Tectonics* 18, 1064–1083. doi: 10.1029/1999TC900040

Cloetingh, S., and Burov, E. B. (2011). Lithospheric folding and sedimentary basin evolution: a review and analysis of formation mechanisms. *Basin Res.* 23, 257–290. doi: 10.1111/j.1365-2117.2010.00490.x

Cloetingh, S., Koptev, A., Kovàcs, I., Gerya, T., Beniest, A., Willingshofer, E., et al. (2021). Plume-induced sinking of intracontinental Lithospheric Mantle: An overlooked mechanism of subduction initiation? *Geochem. Geophys. Geosyst.* 22:e2020GC009482. doi: 10.1029/2020GC009482

Cloetingh, S., Wortel, R., and Vlaar, N. J. (1989). On the initiation of subduction zones. *Pure Appl. Geophys.* 129, 7–25. doi: 10.1007/BF00874622

Cohen, C. R. (1980). Plate tectonic model for the Oligo-Miocene evolution of the western Mediterranean. *Tectonophysics* 68, 283–311. doi: 10.1016/0040-1951(80)90180-8

Cope, M. J. (2003). Algerian licensing round may offer opportunity for exploration plays in deep offshore frontier. *First Break* 21, 37–42. doi: 10.3997/1365-2397.21.7.25550

d'Acremont, E., Lafosse, M., Rabaute, A., Teurquety, G., Do Couto, D., Ercilla, G., et al. (2020). Polyphase tectonic evolution of fore-arc basin related to STEP Fault as revealed by seismic reflection data from the Alboran Sea (W-Mediterranean). *Tectonics* 39:e2019TC005885. doi: 10.1029/2019TC005885

de la Peña, L. G., Ranero, C. R., Gràcia, E., and Booth-Rea, G. (2020). The evolution of the westernmost Mediterranean basins. *Earth Sci. Rev.* 214:103445. doi: 10.1016/j.earscirev.2020.103445

de Lis Mancilla, F., Booth-Rea, G., Stich, D., Pérez-Peña, J. V., Morales, J., Azañón, J. M., et al. (2015). Slab rupture and delamination under the Betics and Rif constrained from receiver functions. *Tectonophysics* 663, 225–237. doi: 10.1016/j.tecto.2015.06.028

de Lis Mancilla, F., Heit, B., Morales, J., Yuan, X., Stich, D., Molina-Aguilera, M., et al. (2018). A STEP fault in Central Betics, associated with lateral lithospheric tearing at the northern edge of the Gibraltar arc subduction system. *Earth Planet. Sci. Lett.* 486, 32–40. doi: 10.1016/j.epsl.2018.01.008

Derder, M. E. M., Djellit, H., Henry, B., Maouche, S., Amenna, M., Bestandji, R., et al. (2019). Strong neotectonic block-rotations, related to the Africa-Eurasia convergence in northern Algeria: paleomagnetic evidence from the Mitidja basin. *Tectonics* 38, 4249–4266. doi: 10.1029/2018TC005394

Déverchère, J., Mercier, De Lépinay, B., Cattaneo, A., Strzerzynski, P., Calais, E., et al. (2010). Comment on "Zemmouri earthquake rupture zone (Mw 6.8, Algeria): aftershocks sequence relocation and 3D velocity model" by A. Ayadi et al. *J. Geophys. Res. Atmos.* 115:B04320. doi: 10.1029/2008JB006190

Déverchère, J., Yelles, K., Domzig, A., Mercier de Lépinay, B., Bouillin, J. P., Gaullier, V., et al. (2005). Active thrust faulting offshore Boumerdes, Algeria, and its relations to the 2003 Mw 6.9 earthquake. *Geophys. Res. Lett.* 32:L04311. doi: 10.1029/2004GL021646

Domzig, A., Gaullier, V., Giresse, P., Pauc, H., Déverchère, J., and Yelles, K. (2009). Deposition processes from echo-character mapping along the western Algerian margin (Oran–Tenes), Western Mediterranean. *Mar. Pet. Geol.* 26, 673–694. doi: 10.1016/j.marpetgeo.2008.05.006

Faccenna, C., Piromallo, C., Crespo-Blanc, A., Jolivet, L., and Rossetti, F. (2004). Lateral slab deformation and the origin of the western Mediterranean arcs. *Tectonics* 23, TC1012. doi: 10.1029/2002TC001488

Fichtner, A., and Villaseñor, A. (2015). Crust and upper mantle of the western Mediterranean – Constraints from full-waveform inversion. *Earth Planet. Sci. Lett.* 428, 52–62. doi: 10.1016/j.epsl.2015.07.038

Frizon de Lamotte, D. (2005). About the Cenozoic inversion of the Atlas domain in North Africa. *C. R. Geosci.* 337, 475–476. doi: 10.1016/j.crte.2005.01.006

Frizon de Lamotte, D., Leturmy, P., Missenard, Y., Khomsi, S., Ruiz, G., et al. (2009). Mesozoic and Cenozoic vertical movements in the Atlas system (Algeria, Morocco, Tunisia): an overview. *Tectonophysics* 475, 9–28. doi: 10.1016/j.tecto.2008.10.024

Frizon de Lamotte, D., Saint Bezar, B., Bracène, R., and Mercier, E. (2000). The two main steps of the Atlas building and geodynamics of the western Mediterranean. *Tectonics* 19, 740–761. doi: 10.1029/2000TC900003

Gaidi, S., Booth-Rea, G., Melki, F., Marzougui, W., Ruano, P., Pérez-Peña, J. V., et al. (2020). Active fault segmentation in Northern Tunisia. *J. Struct. Geol.* 139:104146. doi: 10.1016/j.jsg.2020.104146

Garcia-Castellanos, D., and Cloetingh, S. (2012). "Modeling the interaction between lithospheric and surface processes in foreland basins," in *Tectonics of Sedimentary Basins: Recent Advances*, eds C. Busby and A. Azor (Oxford: Blackwell), 152–181.

Garcia-Castellanos, D., and Villaseñor, A. (2011). Messinian salinity crisis regulated by competing tectonics and erosion at the Gibraltar arc. *Nature* 480, 359–363. doi: 10.1038/nature10651

Gaullier, V., Vendeville, B., Huguen, C., Déverchère, J., Droz, L., Domzig, A., et al. (2006). Role of thick-skinned tectonics on thin-skinned salt tectonics in the western Mediterranean: a comparison between the Algerian and North-Balearic basins. *Geophys. Res. Abstr.* 8:06030.

Giaconia, F., Booth-Rea, G., Ranero, C. R., Gràcia, E., Bartolome, R., Calahorrano, A., et al. (2015). Compressional tectonic inversion of the Algero-Balearic basin: latemost Miocene to present oblique convergence at the Palomares margin (Western Mediterranean). *Tectonics* 34, 1516–1543. doi: 10.1002/2015TC003861

Govers, R., and Wortel, M. J. R. (2005). Lithosphere tearing at STEP faults: response to edges of subduction zones. *Earth Planet. Sci. Lett.* 236, 505–523. doi: 10.1016/j.epsl.2005.03.022

Gràcia, E., Dañobeitia, J., Vergés, J., and Parsifal Team. (2003). Mapping active faults offshore Portugal (36°N–38°N): implications for seismic hazard assessment along the southwest Iberian margin. *Geology* 31, 83–86. doi: 10.1130/0091-7613(2003)031<0083:MAFOPN>2.0.CO;2

Graindorge, D., Sage, F., and Klingelhoefer, F. (2009). SPIRAL Cruise, RV L'Atalante. *French Oceanographic Cruises* doi: 10.17600/9010050

Gueguen, E., Doglioni, C., and Fernandez, M. (1998). On the post 25 Ma geodynamic evolution of the western Mediterranean. *Tectonophysics* 298, 259–269. doi: 10.1016/S0040-1951(98)00189-9

Gurnis, M., Hall, C., and Lavier, L. (2004). Evolving force balance during incipient subduction. *Geochem. Geophys. Geosyst.* 5:Q07001. doi: 10.1029/2003GC000681

Hamai, L., Petit, C., Abtout, A., Yelles-Chaouche, A., and Déverchère, J. (2015). Flexural behaviour of the north Algerian margin and tectonic implications. *Geophys. J. Int.* 201, 1426–1436. doi: 10.1093/gji/ggv098

Hamai, L., Petit, C., Le Pourhiet, L., Yelles-Chaouche, A., Déverchère, J., Beslier, M. O., et al. (2018). Towards subduction inception along the inverted North African margin of Algeria? Insights from thermo-mechanical models. *Earth Planet. Sci. Lett.* 501, 13–23. doi: 10.1016/j.epsl.2018.08.028

Hidas, K., Garrido, C. J., Booth-Rea, G., Marchesi, C., Bodinier, J. L., Dautria, J. M., et al. (2019). Lithosphere tearing along STEP faults and synkinematic formation of lherzolite and wehrlite in the shallow subcontinental mantle. *Solid Earth* 10, 1099–1121. doi: 10.5194/se-2019-32

Iacopini, D., Butler, R. W. H., Purves, S., McArdlec, N., and De Freslon, N. (2016). Exploring the seismic expression of fault zones in 3D seismic volumes. *J. Struct. Geol.* 89, 54–73. doi: 10.1016/j.jsg.2016.05.005

Japsen, P., Chalmers, J. A., Green, P. F., and Bonow, J. M. (2012). Elevated, passive continental margins: not rift shoulders, but expressions of episodic, post-rift burial and exhumation. *Glob. Planet. Change.* 90–91, 73–86. doi: 10.1016/j.gloplacha.2011.05.004

Jolivet, L., and Faccenna, C. (2000). Meditterranean extension and the Africa-Eurasia collision. *Tectonics* 19, 1095–1106. doi: 10.1029/2000TC900018

Kherroubi, A., Déverchère, J., Yelles, A., Mercier de Lépinay, B., Domzig, A., Cattaneo, A., et al. (2009). Recent and active deformation pattern off the easternmost Algerian margin, Western Mediterranean Sea: new evidence for contractional tectonic reactivation. *Mar. Geol.* 261, 17–32. doi: 10.1016/j.margeo.2008.05.016

Kherroubi, A., Yelles-Chaouche, A., Koulakov, I., Déverchère, J., Beldjoudi, H., Haned, A., et al. (2017). Full Aftershock Sequence of the M w 6.9 2003 Boumerdes Earthquake, Algeria: space–time distribution, local tomography and Seismotectonic implications. *Pure Appl. Geophys.* 174, 2495–2521. doi: 10.1007/s00024-017-1571-5

Khomsi, S., Roure, F., Khelil, M., Mezni, R., and Echihie, O. (2019). A review of the crustal architecture and related pre-salt oil/gas objectives of the eastern Maghreb Atlas and Tell: need for deep seismic reflection profiling. *Tectonophysics* 766, 232–248. doi: 10.1016/j.tecto.2019.06.009

Kim, G. B., Yoon, S. H., Kim, S. S., and So, B. D. (2018). Transition from buckling to subduction on strike-slip continental margins: evidence from the East Sea (Japan Sea). *Geology* 46, 603–606. doi: 10.1130/G40305.1

Leprêtre, A. (2012). *Contraintes par imagerie sismique pénétrante sur l'évolution d'une marge Cénozoïque réactivée en compression*. Ph.D. thesis. Brest, Université de Bretagne Occidentale, 236.

Leprêtre, A., Klingelhoefer, F., Graindorge, D., Schnurle, P., Yelles, K., Déverchère, J., et al. (2013). Multiphased tectonic evolution of the Central Algerian margin from combined wide-angle and reflection seismic data off Tipaza, Algeria. *J. Geophys. Res. Solid Earth* 118, 3899–3916. doi: 10.1002/jgrb.50318

Leroy, M., Dauteuil, O., and Cobbold, P. R. (2004). Incipient shortening of a passive margin: the mechanical roles of continental and oceanic lithospheres. *Geophys. J. Int.* 159, 400–411. doi: 10.1111/j.1365-246X.2004.02400.x

Lofi, J., Déverchère, J., Gaullier, V., Gillet, H., Gorini, C., Guennoc, P., et al. (2011a). *Seismic Atlas of the Messinian Salinity Crisis markers in the Mediterranean and Black Seas*. Paris: CGMW.

Lofi, J., Sage, F., Déverchère, J., Loncke, L., Maillard, A., Gaullier, V., et al. (2011b). Refining our knowledge of the Messinian salinity crisis records in the offshore domain through multi-site seismic analysis. *Bull. Soc. Geol. France* 182, 163–180. doi: 10.2113/gssgfbull.182.2.163

Manighetti, I., Campillo, M., Bouley, S., and Cotton, F. (2007). Earthquake scaling, fault segmentation, and structural maturity. *Earth Planet. Sci. Lett.* 253, 429–438. doi: 10.1016/j.epsl.2006.11.004

Martínez-García, P., Soto, J. I., and Comas, M. (2011). Recent structures in the Alboran Ridge and Yusuf fault zones based on swath bathymetry and sub-bottom profiling: evidence of active tectonics. *Geo Mar. Lett.* 31, 19–36. doi: 10.1007/s00367-010-0212-0

Matias, H., Kress, P., Terrinha, P., Mohriak, W., Menezes, P., Matias, L., et al. (2011). Salt tectonics in the Western Gulf of Cadiz, southwest Iberia. *AAPG Bull.* 95, 1667–1698. doi: 10.1306/01271110032

Mauffret, A. (2007). The Northwestern (Maghreb) boundary of the Nubia (Africa) plate. *Tectonophysics* 429, 21–44. doi: 10.1016/j.tecto.2006.09.007

Mauffret, A., Frizon, de Lamotte, F., Lallemant, S., Gorini, C., and Maillard, A. (2004). E–W opening of the Algerian Basin (Western Mediterranean). *Terra Nova* 16, 257–264. doi: 10.1111/j.1365-3121.2004.00559.x

McKenzie, D. P. (1977). "Initiation of trenches: a finite amplitude instability," in *Island Arcs, Deep Sea Trenches and Back-Arc Basins, Maurice Ewing Series, 1*, eds M. Talwani, and W. C. Pittman (Washington, DC: American Geophysical Union), 57–62. doi: 10.1029/ME001p0057

Medaouri, M. (2014). *Origine de la segmentation de la marge Algérienne et implication sur l'évolution géodynamique et les ressources pétrolières*. Ph.D. thesis. Brest, Université de Bretagne Occidentale, 254.

Medaouri, M., Bracene, R., Déverchère, J., Graindorge, D., Ouabadi, A., and Yelles-Chaouche, A. (2012). Structural styles and Neogene petroleum system around the Yusuf-Habibas ridge (Alboran basin, Mediterranean sea). *Lead. Edge* 31, 776–785. doi: 10.1190/tle31070776.1

Medaouri, M., Déverchère, J., Graindorge, D., Bracène, R., Badji, R., Ouabadi, A., et al. (2014). The transition from Alboran to Algerian basins (Western Mediterranean Sea): chronostratigraphy, deep crustal structure and tectonic evolution at the rear of a narrow slab rollback system. *J. Geodyn.* 77,186–205. doi: 10.1016/j.jog.2014.01.003

Meghraoui, M. (1991). Blind reverse faulting system associated with the Mont Chenoua-Tipaza earthquake of 29 October 1989 (north-central Algeria). *Terra Nova* 3, 84–92. doi: 10.1111/j.1365-3121.1991.tb00847.x

Meghraoui, M., and Pondrelli, S. (2012). Active faulting and transpression tectonics along the plate boundary in North Africa. *Ann. Geophys.* 55, 955–967. doi: 10.4401/ag-4970

Mihoubi, A. (2014). *Imagerie sismique de la structure profonde de la marge Algérienne orientale (secteur de Jijel) - implications en termes de potentiel pétrolier*. Ph.D. thesis. Brest, Université de Bretagne Occidentale, 178.

Mihoubi, A., Schnurle, P., Benaissa, Z., Badsi, M., Bracene, R., Djelit, H., et al. (2014). Seismic imaging of the eastern Algerian margin off Jijel: integrating wide-angle seismic modelling and multichannel seismic pre-stack depth migration. *Geophys. J. Int.* 198, 1486–1503. doi: 10.1093/gji/ggu179

Morellato, C., Redini, F., and Doglioni, C. (2003). On the number and spacing of faults. *Terra Nova* 15, 315–321. doi: 10.1046/j.1365-3121.2003.00501.x

Nikolaeva, K., Gerya, T. V., and Marques, F. O. (2010). Subduction initiation at passive margins: numerical modeling. *J. Geophys. Res.* 115:B03406. doi: 10.1029/2009JB006549

Ousadou, F., and Bezzeghoud, M. (2019). "Seismicity of the Algerian Tell Atlas and the Impacts of major earthquakes," in *The Geology of the Arab World—An Overview, Springer Geology*, eds A. Bendaoud, Z. Hamimi, M. Hamoudi, S. Djemai, and B. Zoheir (Cham: Springer), 401–426. doi: 10.1007/978-3-319-96794-3_11

Park, J. O., Tsuru, T., Kodaira, S., Cummins, P. R., and Kaneda, Y. (2002). Splay fault branching along the Nankai subduction zone. *Science* 297, 1157–1160. doi: 10.1126/science.1074111

Pedoja, K., Husson, L., Regard, V., Robert Cobbold, P., Ostanciaux, E., Johnson, M. E., et al. (2011). Relative sea-level fall since the last interglacial stage: Are coasts uplifting worldwide? *Earth Sci. Rev.* 108, 1–15. doi: 10.1016/j.earscirev.2011.05.002

Perea, H., Gràcia, E., Martínez-Loriente, S., Bartolome, R., de la Peña, L. G., de Mol, B., et al. (2018). Kinematic analysis of secondary faults within a distributed shear-zone reveals fault linkage and increased seismic hazard. *Mar. Geol.* 399, 23–33. doi: 10.1016/j.margeo.2018.02.002

Piqué, A., Aït Brahim, L., El Azzouzi, M., Maury, R. C., Bellon, H., Semroud, B., et al. (1998). The Maghreb indenter: structural and chemical data. *C.R. Acad. Sci. Ser. IIA Earth Planet. Sci.* 326, 575–581.

Poort, J., and Et, A. L. (2020). Heat flow in the Western Mediterranean: thermal anomalies on the margins, the seafloor and the transfer zones. *Mar. Geol.* 419:106064. doi: 10.1016/j.margeo.2019.106064

Rabaute, A., and Chamot-Rooke, N. (2015). *Active tectonics of the Africa-Eurasia Boundary from Algiers to Calabria. Map at 1: 500 000 Scale*. Paris: Geosubsight. doi: 10.13140/RG.2.2.23493.86245

Ratzov, G., Cattaneo, A., Babonneau, N., Déverchère, J., Yelles, K., Bracene, R., et al. (2015). Holocene turbidites record earthquake supercycles at slow rate plate boundary. *Geology* 43, 331–334. doi: 10.1130/G36170.1

Roure, F., Casero, P., and Addoum, B. (2012). Alpine inversion of the North African margin and delamination of its continental lithosphere. *Tectonics* 31:TC3006. doi: 10.1029/2011TC002989

Sibuet, J. C., He, E., Zhao, M., Pang, X., and Klingelhoefer, F. (2019). Oceanic mantle reflections in deep seismic profiles offshore Sumatra are faults or fakes. *Sci. Rep.* 9:13354. doi: 10.1038/s41598-019-49607-x

Soto, J., Déverchère, J., Medaouri, M., and Leffondré, P. (2018). "The Messinian salt layer squeezed by active plate convergence in the western Mediterranean margins," in *Poster at the AAPG Workshop in GTW Series, Alpine Folded Belts and Extensional Basins*, Granada.

Soumaya, A., Ben Ayed, N., Rajabi, M., Meghraoui, M., Delvaux, D., Kadri, A., et al. (2018). Active faulting geometry and stress pattern near complex strike-slip systems along the Maghreb Region: constraints on active convergence in the Western Mediterranean. *Tectonics* 37, 3148–3173. doi: 10.1029/2018TC004983

Stein, C. A., Cloetingh, S., and Wortel, R. (1989). Seasat-derived gravity constraints on stress and deformation in the northeastern Indian Ocean. *Geophys. Res. Lett.* 16, 823–826. doi: 10.1029/GL016i008p00823

Stern, R. J. (2004). Subduction initiation: spontaneous and induced. *Earth Planet. Sci. Lett.* 226, 275–292. doi: 10.1016/j.epsl.2004.08.007

Stern, R. J., and Gerya, T. V. (2018). Subduction initiation in nature and models: a review. *Tectonophysics* 746, 173–198. doi: 10.1016/j.tecto.2017.10.014

Stirling, M., Goded, T., Berryman, K., and Litchfield, N. (2013). Selection of Earthquake scaling relationships for seismic-hazard analysis. *Bull. Seismol. Soc. Am.* 103, 2993–3011. doi: 10.1785/0120130052

Strasser, M., Moore, G., Kimura, G., Kitamura, Y., Kopf, A. J., Lallement, S., et al. (2009). Origin and evolution of a splay fault in the Nankai accretionary wedge. *Nat. Geosci.* 2, 648–652. doi: 10.1038/ngeo609

Strzerzynski, P., Déverchère, J., Cattaneo, A., Domzig, A., Yelles, K., Mercier, et al. (2010). Tectonic inheritance and Pliocene-Pleistocene inversion of the Algerian margin around Algiers: insights from multibeam and seismic reflection data. *Tectonics* 29:TC2008. doi: 10.1029/2009tc002547

Strzerzynski, P., Dominguez, S. É., Boudiaf, A., and Déverchère, J. (2021). Tectonic inversion and geomorphic evolution of the Algerian margin since Messinian times: insights from new onshore/offshore analog modeling experiments. *Tectonics* 40:e2020TC006369. doi: 10.1029/2020TC006369

Sulli, A., Morticelli, M. G., Agate, M., and Zizzo, E. (2021). Active north-vergent thrusting in the northern Sicily continental margin in the frame of the quaternary evolution of the Sicilian collisional system. *Tectonophysics* 802:228717. doi: 10.1016/j.tecto.2021.228717

Tavani, S., Storti, F., Lacombe, O., Corradetti, A., Muñoz, J. A., and Mazzoli, S. (2015). A review of deformation pattern templates in foreland basin systems and fold-and-thrust belts: implications for the state of stress in the frontal regions of thrust wedges. *Earth Sci. Rev.* 141, 82–104. doi: 10.1016/j.earscirev.2014.11.013

Thorwart, M., Dannowski, A., Grevemeyer, I., Lange, D., Kopp, H., Petersen, F., et al. (2021). Basin inversion: reactivated rift structures in the Ligurian Sea revealed by OBS. *Solid Earth Discuss.* [Preprint]. doi: 10.5194/se-2021-9

Totake, Y., Butler, R. W. H., and Bond, C. E. (2017). Structural validation as an input into seismic depth conversion to decrease assigned structural uncertainty. *J. Struct. Geol.* 95, 32–47. doi: 10.1016/j.jsg.2016.12.007

U.S. Geological Survey (2021). *Earthquake Catalog*. Available online at: https://earthquake.usgs.gov/earthquakes/search/ (accessed February 18, 2021).

van Hinsbergen, D. J. J., Torsvik, T. H., Schmid, S. M., Maţenco, L. C., Maffione, M., Vissers, R. L. M., et al. (2020). Orogenic architecture of the Mediterranean region and kinematic reconstruction of its tectonic evolution since the Triassic. *Gondwana Res.* 81, 79–229. doi: 10.1016/j.gr.2019.07.009

van Hinsbergen, D. J. J., Vissers, R. L. M., and Spakman, W. (2014). Origin and consequences of western Mediterranean subduction, rollback, and slab segmentation. *Tectonics* 33, 393–419. doi: 10.1002/tect.20125

Wells, D. L., and Coppersmith, K. J. (1994). New empirical relationships among magnitude, rupture length, rupture width, rupture area, and surface displacement. *Bull. Seismol. Soc. Am.* 84, 974–1002.

Yamato, P., Husson, L., Becker, T. W., and Pedoja, K. (2013). Passive margins getting squeezed in the mantle convection vice. *Tectonics* 32, 1559–1570. doi: 10.1002/2013TC003375

Yelles, K., Domzig, A., Déverchère, J., Bracene, R., Mercier, de Lépinay, B., et al. (2009). Plio-Quaternary reactivation of the Neogene margin off NW Algiers, Algeria: the Khayr al Din bank. *Tectonophysics* 475, 98–116. doi: 10.1016/j.tecto.2008.11.030

Yelles-Chaouche, A. K., Abacha, I., Boulahia, O., Aidi, C., Chami, A., Belheouane, A., et al. (2021). The 13 July 2019 Mw 5.0 Jijel Earthquake, northern Algeria: an indicator of active deformation along the eastern Algerian margin. *J. Afr. Earth Sci.* 177:104149. doi: 10.1016/j.jafrearsci.2021.104149

Yelles-Chaouche, A. K., Boudiaf, A., Djellit, H., and Bracene, R. (2006). Tectonique active de la région nord-algérienne. *Geoscience* 338, 126–139. doi: 10.1016/j.crte.2005.11.002

Yelles-Chaouche, A. K., Kherroubi, A., and Beldjoudi, H. (2017). The large Algerian earthquakes (267 A.D.-2017). *Fis. Tierra* 29, 159–182. doi: 10.5209/FITE.57617

Yelles-Chaouche, A. K., Roger, J., Déverchère, J., Bracene, R., Domzig, A., Hebert, H., et al. (2009). The 1856 Tsunami of Djidjelli (Eastern Algeria): seismotectonics modelling and hazard implications for the Algerian Coast. *Pure Appl. Geophys.* 166, 283–300. doi: 10.1007/s00024-008-0433-6

Zitellini, N., Ranero, C. R., Loreto, M. F., Ligi, M., Pastore, M., D'Oriano, F., et al. (2020). Recent inversion of the Tyrrhenian Basin. *Geology* 48, 123–127. doi: 10.1130/G46774.1

Conflict of Interest: MM and MA were employed by the company Sonatrach/Exploration Division.

The remaining authors declare that the research was conducted in the absence of any commercial or financial relationships that could be construed as a potential conflict of interest.